Journal of Power Sources 195 (2010) 4470–4493

Contents lists available at ScienceDirect

Journal of Power Sources

journal homepage: www.elsevier.com/locate/jpowsour

Optimization studies of carbon additives to negative active material for the purpose of extending the life of VRLA batteries in high-rate partial-state-of-charge operation

D.P. Boden*, D.V. Loosemore, M.A. Spence, T.D. Wojcinski

Hammond Expanders Division, Hammond Group, Inc., 6544 Osborn Avenue, Hammond, IN 46320, USA

ARTICLE INFO

Article history:
Received 9 November 2009
Received in revised form
15 December 2009
Accepted 16 December 2009
Available online 23 December 2009

Keywords:
Lead-acid batteries
Negative electrodes
Cycle life
Carbon additives
High-rate charging

ABSTRACT

The negative plates of lead-acid batteries subjected to partial-state-of-charge (PSOC) operation fail because of the development of an electrically inert film of lead sulfate on their surfaces. It has been found that carbon additives to the negative active material can significantly increase their cycle life in this type of operation. In this paper we show that various types of carbon, including graphite, carbon black eliminate the surface development of lead sulfate and that, in their presence, the lead sulfate becomes homogeneously distributed throughout the active material. Examination of active material by energy dispersive spectroscopy after extensive cycling shows that lead formed during charge of lead sulfate preferentially deposits on the carbon particles that have been embedded in the active material. Electrochemical studies have been carried out on a number of types of carbon additives having a wide range of properties. These included flake, expanded and synthetic graphite, isotropically graphitized carbon, carbon black and activated carbon. We have investigated their effect on the resistivity and surface areas of the negative active material and also on such electrochemical properties as active material utilization and cycle life. Most of the carbon additives increase the utilization of the active material and impressive increases in cycle life have been obtained with over 6000 capacity turnovers having been achieved. However, at this time, we have not been able to correlate either the type or the properties of the carbon with capacity or cycle life. Further work is needed in this area. The increases that have been achieved in cycle life provide evidence that the lead-acid battery is a viable low cost option for hybrid-electric vehicle use.

1. Introduction

When VRLA batteries are used in a partial-state-of-charge (PSOC) mode, as in hybrid electric vehicles, an electrochemically passive film of lead sulfate is formed on the surface of the negative plates [1]. This becomes thicker with further cycling and causes a progressive reduction of capacity leading to premature failure. Furthermore, this film cannot be reduced to lead by conventional recovery cycling. Interestingly, this finding is one of the few instances where lead-acid battery life is limited by the negative electrode. This phenomenon does not occur in the positive plate nor does it appear to be a function of oxygen reduction since it also occurs in flooded batteries [2].

Recent work, primarily supported by the Advanced Lead-Acid Battery Consortium (ALABC) [3] has shown that this problem can be eliminated by addition of higher than usual levels of carbon to the negative active material. Different types of carbon have been found to be effective such as carbon black and graphite. This work has been confirmed by battery manufacturers in full-sized, commercially built batteries [4] where cycle lives of up to 300,000 PSOC cycles have been achieved. Without the carbon additives the life is reduced to only 25,000 cycles.

The reasons why carbon is so effective are not understood. This may be because there has been no organized, systematic study of how the various chemical and physical properties of carbons affect PSOC cycle life. This is understandable since the beneficial effects have only recently been discovered and there are many forms of carbon (carbon black, activated carbon, graphite, etc.) whose properties span a wide range of physical differences, making it a lengthy task to investigate all of them. Additionally, within each class of carbon there are wide ranges of properties. For example different types of carbon black show wide ranges of:

* Corresponding author at: 1661 Brown's Gap Turnpike, Charlottesville, VA 22901, USA. Tel.: +1 434 823 5036/219 989 4060x753; fax: +1 434 823 5806.
E-mail addresses: dpboden@yahoo.com, dboden@hmndexpander.com (D.P. Boden).

0378-7753/$ – see front matter © 2009 Elsevier B.V. All rights reserved.
doi:10.1016/j.jpowsour.2009.12.069

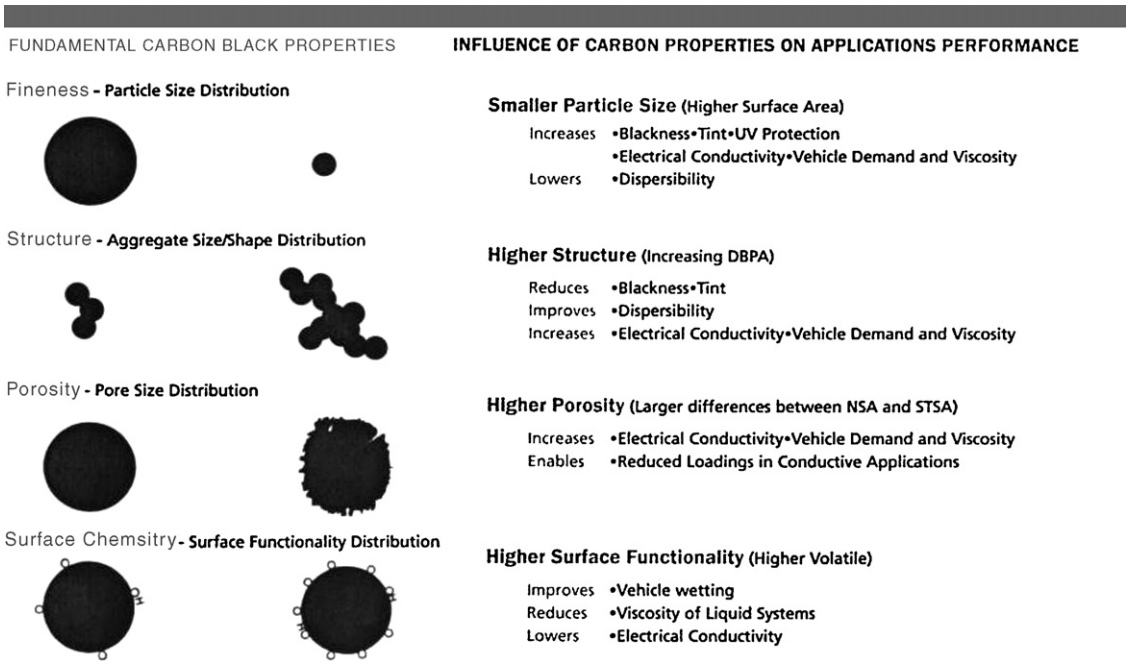

Fig. 1. Influence of carbon black properties on function. DBPA: dibutyl phthalate absorption; NSA: nitrogen surface area (BET); STSA: statistical thickness surface area.

- particle size distribution;
- aggregate size and shape (structure);
- surface area;
- electrical conductivity;
- porosity;
- surface functionality.

Each of these properties, either separately or in combination, may have an influence on the electrochemical behavior of the negative plate. Some of these influences are shown in Fig. 1.

There are also several types of graphite, some of which have already been evaluated [5]. These include natural flake, synthetic and expanded varieties. Differences in cycle life have been reported from these materials [6].

Activated carbons, although not presently used in lead-acid batteries, have also been considered as candidate materials since they possess properties that promote reactions on their surfaces. An example of this is their use in catalytic converters in automobiles. Recent unpublished work, carried out in our laboratories, has shown that they also have the capacity to improve cycle life in PSOC operation.

Before a specification for carbon can be defined, there must be improved understanding of how the different types, and variations within those types, influence the behavior of negative electrodes in PSOC operation. Fortunately, previous work has yielded important clues, particularly that certain forms of graphite and carbon black are very effective in improving PSOC cycle life. We now need to define the critical characteristics of these materials so that the optimum choice can be made for the VRLA battery in hybrid electric vehicles.

Scholz et al. [7,8] have suggested that direct electrochemical reduction of lead compounds in hydrochloric acid can take place in the solid state on graphite paste electrodes and that the reduction takes place through epitactic solid state conversion without any dissolved intermediates. A similar mechanism may occur during reduction of lead sulfate in sulfuric acid. More recently Pavlov et al. [9] have proposed that electrochemical reduction of lead ions to lead in sulfuric acid takes place preferentially on the surface of electrochemically active carbon. The beneficial properties of carbon make it worthwhile to carry out further work to optimize its properties and to elucidate the mechanism by which it increases PSOC cycle life.

This paper describes a program of work to evaluate several types of carbon, including graphite, activated carbon and carbon black in the negative electrodes of VRLA batteries undergoing PSOC cycling to determine which properties are the most important in achieving long service life. It involves determining the effects of these materials on the conductivity of lead sulfate and NAM, electrochemical testing and studying the effects of the materials on the morphology of the active material before, during and after cycling.

2. Experimental approach

Two separate studies have been carried out. In the first of these (Task 1), only two types of carbon were studied, carbon black and purified natural flake graphite. The carbon materials that were selected are shown in Table 1 with some of their physical properties.

The carbon black was chosen because of its relatively high specific surface area, long chain length and small particle size while

Table 1
Selected physical properties of carbon additives used in Task 1 studies.

Additive	Surface area ($m^2\ g^{-1}$)	Mean particle size	Conductivity ($\Omega^{-1}\ cm^{-1}$)	Supplier
Carbon black Grade: N134	143	18 nm	100	S. D. Richardson Company, 3560 W. Market Street, Suite 420, Akron, OH 44333, USA
Purified Flake Graphite Grade: 2939APH	9	28 μm	100	Superior Graphite Co., 4201 W. 36th Street, Chicago, IL 60632, USA

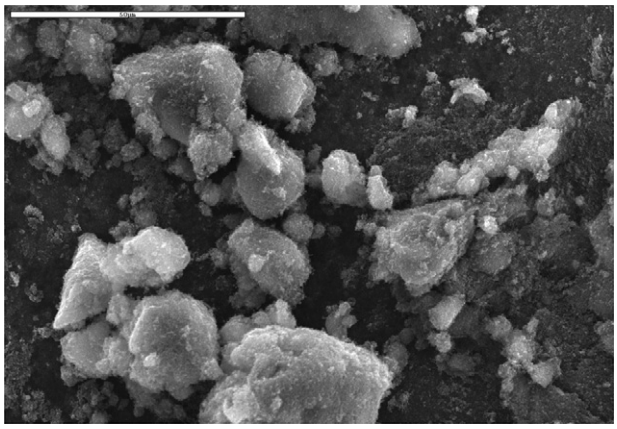

Fig. 2. SEM image of N134 carbon black. Magnification: 1000×.

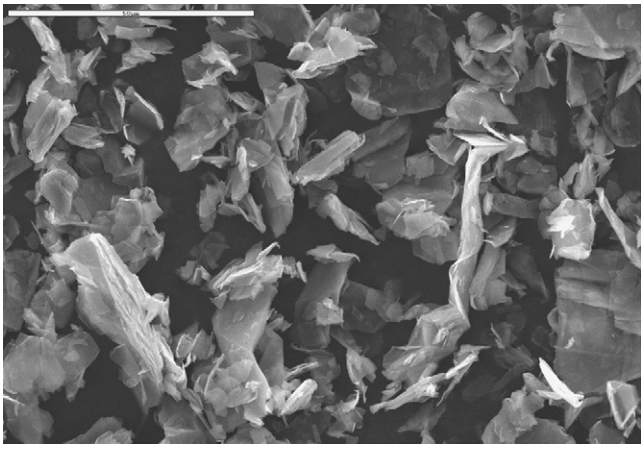

Fig. 3. SEM image of 2939APH graphite. Magnification: 1000×.

the graphite was chosen because it had shown encouraging properties in ALABC Project N 1.2 and is used in lithium-ion battery electrodes.

SEM images of the carbon black and graphite are shown in Figs. 2 and 3. As can be seen in Fig. 2 the N134 carbon black is pelletized in the non-milled form. The extent to which the granules are broken down with milling during preparation of the test mixtures is unknown since carbon black cannot be identified by SEM. These materials were added to the negative active material as components of expanders having the compositions shown in Table 2.

2.1. Preparation of test mixtures

Before preparation of the test mixtures the carbon black was milled in a ball mill for 30 min to break down the pellets. The additive mixtures were prepared by weighing the materials into containers and then ball milling for a further 30 min. In the cases where only one component was involved no ball milling was carried out. These additive mixtures were used to make experimental paste batches of 22.7 kg using a conventional negative paste formula. The experimental plan for the additive mixtures is shown in Table 3.

Table 2
Compositions of additives to the negative active material.

Additive	Concentration in NAM (by weight)		
Barium sulfate	0.8%		
Vanisperse A	0.2%	0.4%	0.6%
Carbon black	0	1%	2%
Graphite	0	1%	2%

In every case we were able to make paste successfully, using a Wirtz orifice pasting machine and pasting paper, although the paste characteristics were significantly changed in a number of cases, particularly in those pastes containing large amounts of additive. Variable amounts of water were added and paste mixing times were adjusted to produce material that could be pasted. Although all the paste mixes could be pasted, sometimes with difficulty, it is clear that considerable changes to paste formulations and to pasting processes will be necessary when high dosage levels of carbon additives are used.

The BET surface areas of the additive blends and the formed negative plates and their average weights are shown in Table 4.

A wide range of surface areas is observed depending on the composition of the additive and, as expected, additive mixtures with the highest surface area give higher surface area negative active material. Plate weights can be seen to vary from 54.86 to 49.12 g. The lowest weight was obtained from Run 1 which contained the greatest amount of carbon additive (4%). This probably reflects the amount of water that had to be added to make the paste workable.

2.2. Electrochemical testing

The electrodes were assembled into the three-plate VRLA cells (two positives and one negative) shown in Fig. 4. These cells were designed to hold the electrodes in the horizontal position to eliminate the possibility of electrolyte stratification and were strongly negative limited with 4.35 and 1.74 Ah of positive and negative capacity respectively at the *C*/1 rate. They were formed using a formation protocol provided by the plate manufacturer, NorthStar Battery Company. These cells were cycled with the same PSOC protocol used previously by Hollenkamp and Newnham in ALABC projects N 1.2 and C/N 1.1. This was done to ensure that our data could be compared to that obtained previously. The NAM was characterized before and after cycling using EMP, XRD, cathodoluminescence and BET surface area measurements

The test protocol is shown in Table 5. Steps 4–8 are termed a cycle set. Since a unity charge factor is used in these steps the amount of charge accepted by the negative plate is slightly lower than the amount of charge removed by the previous discharge step. Therefore the capacity declines gradually due to accumulation of lead sulfate. The number of cycles achieved in a cycle set, therefore, is a measure of the charge acceptance of the electrode. The

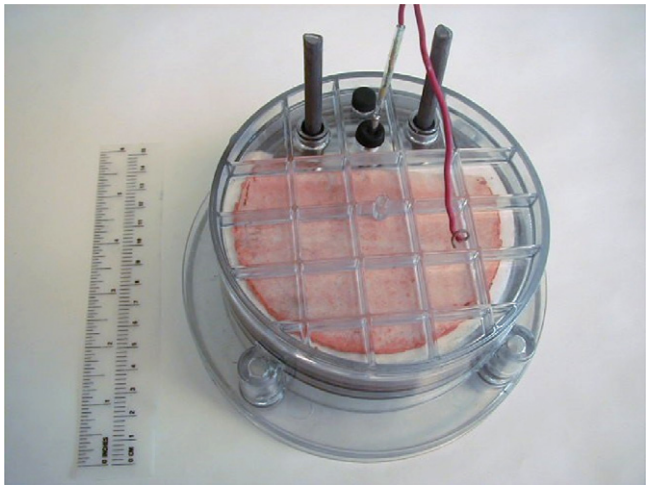

Fig. 4. Fixture for electrochemical evaluation of negative plates containing additive mixtures.

Table 3
Experimental plan for carbon additive mixes. Percentage loading and weights are for a 22.7 kg paste batch.

Run	Barium sulfate		Vanisperse A		Carbon black N134		Graphite 2939APH	
	%	g	%	g	%	g	%	g
1	0.8	181.44	0.6	136.08	2	453.6	2	453.6
2	0.8	181.44	0.2	45.36	0	0	2	453.6
3	0.8	181.44	0.6	136.08	0	0	0	0
4	0.8	181.44	0.2	45.36	2	453.6	2	453.6
5	0.8	181.44	0.6	136.08	0	0	2	453.6
6	0.8	181.44	0.2	45.36	0	0	0	0
7	0.8	181.44	0.6	136.08	2	453.6	0	0
8	0.8	181.44	0.2	45.36	2	453.6	0	0

Table 4
BET surface areas of additive blends, BET surface areas of formed negative plates and plate weights.

Run	BETSA of additive blend ($m^2\ g^{-1}$)	BETSA of formed negative plate[1] ($m^2\ g^{-1}$)	Plate weight (g)
1	77.95	3.28	49.12
2	22.43	1.23	51.20
3	0.17	1.36	50.97
4	84.33	3.11	50.42
5	10.29	1.61	51.20
6	0.17	1.00	52.35
7	124.57	2.99	54.24
8	147.04	2.93	54.86

recovery charge at the end of a cycle set measures the effectiveness of the additives in facilitating reduction of the accumulated lead sulfate to lead. Cycle sets are repeated until the capacity following a recovery cycle has dropped to 70% of its initial value. The total number of cycles obtained before the capacity has fallen to 70% is designated as the cycle life.

2.3. Capacity testing

Results from the initial capacity tests are shown in Fig. 5.

The blue bars show the initial capacity obtained after 10 conditioning cycles while the red bars show the peak capacity reached during cycling. These data have been expressed as mAh g^{-1} to take account of the different active material weights in the plates as a result of various concentrations of additive. Each data point represents the average of four cells. In test groups 1, 2, 3, 4, 5 and 6 the capacity increased during cycling before declining at the end of life while the capacities of test groups 7 and 8 declined from the start. Groups 1, 2, 4, 5, 7 and 8 contained carbon black and/or graphite as a conductive additive while test groups 3 and 6 contained no carbon additives.

2.4. Cycle life testing

Cycle life data are shown in Fig. 6. Groups 1, 2 and 4 achieved the longest cycle lives, 109,461, 149,116 and 139,570 respectively. Following failure, the cells from Runs 1, 2 and 4 were taken apart and examined. It was found that the cells were dry, indicating loss of water during cycling. Furthermore, the cell from Group 4 had a severely corroded contact. These observations showed that the primary causes of failure were from factors not associated with sulfation. The cells were rebuilt with the original plates and new separators, were filled with 1.280 s g. sulfuric acid and then placed back on cycling. Considerable recovery of the capacity was obtained showing that the negative plates were still serviceable. Clearly, much longer cycle lives should be expected from commercially produced cells with better seals and valve design.

The compositions of the additives in tests 1, 2 and 4 are:

Run 1: Vanisperse A—0.6%, Carbon black N134—2.0%, Graphite 2939APH—2.0%
Run 2: Vanisperse A—0.2%, Carbon black N134—0, Graphite 2939APH—2.0%
Run 4: Vanisperse A—0.2%, Carbon black N134—2%, Graphite 2939APH—2.0%.

An obvious feature of these data is that the best performing additive mixtures all contained 2% graphite 2939APH although test group 5, which also contained graphite, only achieved 6276 cycles. We attribute this an assembly defect. Test group 6, which achieved 8517 cycles, is very similar to a standard commercial expander commonly used in VRLA batteries. This can be considered as a control test. The increase in PSOC life as a result of the addition of higher levels of carbon to the plates is very significant.

2.5. Examination of cycled plates

Plates were removed from cells according to the protocol described in Table 6, step 9 and were washed in distilled water and dried at 110 °C. They were examined by X-ray diffraction (XRD), scanning electron microscopy (SEM) and an electron microprobe (EMP). Identification of phases by XRD was done by comparison with a library of standard patterns while the amount of each phase was determined by intensity comparison with weighed

Table 5
HRPOC cycling procedure.

Step	Procedure
1	Cell formation using NorthStar Battery Company procedure.
2	Capacity test at *C*/1 rate (1.74 A). Recharge and repeat for 10 cycles.
3	Recharge to 100% SOC. Remove one cell of each variable for physical/chemical characterization.
4	Discharge to 50% SOC at *C*/1 rate (0.87 Ah).
5	Cycle at 2*C* rate (3.48 A); discharge 60 s, rest 10 s, charge 60 s, rest 10 s.
6	Cycle until end-of-discharge voltage ≤1.70 vpc
7	Recharge to 100% state-of-charge
8	Capacity test at *C*/1 rate and recharge.
9	Remove one cell of each variable for physical/chemical characterization when capacity has dropped to 90%, 80% and 70% of initial value

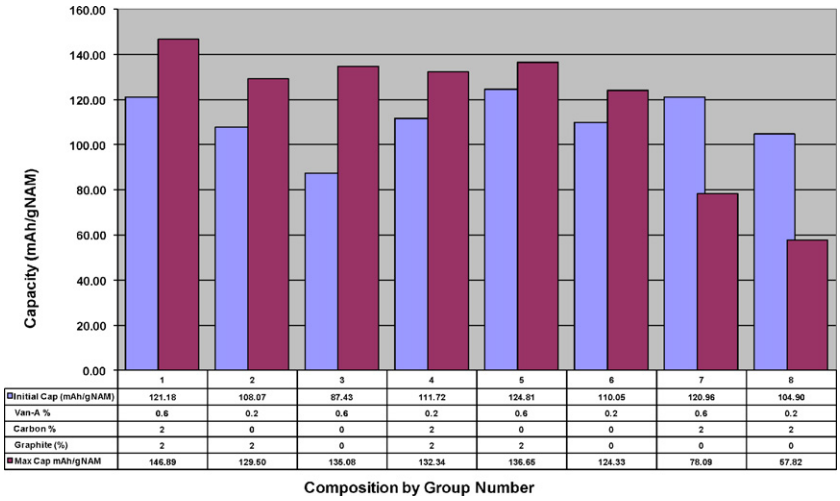

	1	2	3	4	5	6	7	8
Initial Cap (mAh/gNAM)	121.18	108.07	87.43	111.72	124.81	110.05	120.96	104.90
Van-A %	0.6	0.2	0.6	0.2	0.6	0.2	0.6	0.2
Carbon %	2	0	0	2	0	0	2	2
Graphite (%)	2	2	0	2	2	0	0	0
Max Cap mAh/gNAM	146.89	129.50	135.08	132.34	136.65	124.33	78.09	57.82

Fig. 5. Initial capacity data from cells with carbon additives.

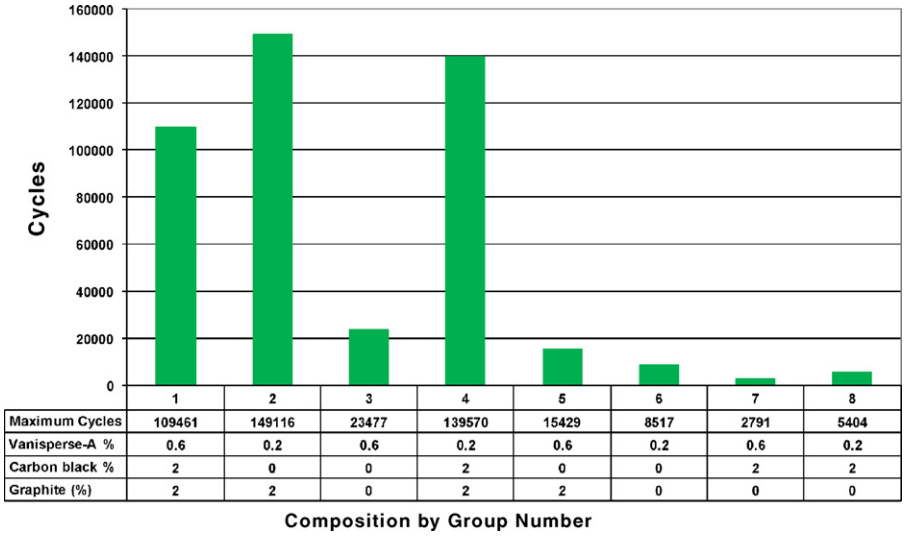

	1	2	3	4	5	6	7	8
Maximum Cycles	109461	149116	23477	139570	15429	8517	2791	5404
Vanisperse-A %	0.6	0.2	0.6	0.2	0.6	0.2	0.6	0.2
Carbon black %	2	0	0	2	0	0	2	2
Graphite (%)	2	2	0	2	2	0	0	0

Fig. 6. Cycle life of cells with carbon black and graphite additives.

mixtures simulating the approximate unknown compositions. The samples were prepared by grinding the NAM to a powder.

SEM was used to obtain images of samples that showed the morphology, size, surface roughness, pore structure and the chemical identification of individual grains. Generally, rough samples were used which were imaged at magnifications ranging from 50× to 100,000×.

The different magnifications showed different features of the sample. The usual technique was used of observing the sample in vacuum after a conducting coating was added. The instrument used was a filament-source JEOL JSM-5800LV. This machine allowed digital imaging to about 6000×. An energy dispersive (EDS) X-ray detector incorporating a thin-window allowed identification of all elements (C and heavier) within any phase within the image with an analytical volume of several microns. X-ray imaging of flat,

Table 6
Properties of graphite materials used in Task 2.

Additive	BET specific surface area ($m^2\ g^{-1}$)	Mean particle size, D_{50} (μm)	Supplier	Degree of crystallinity (Lc nm)	Interlayer distance (nm)	Description
Graphite 2939APH	7.72	10.0	Superior Graphite Co.	>200	0.3355	Purified natural flake graphite
Graphite AGB1010	23.5	9.8	Superior Graphite Co.	~40	0.3355	Purified expanded graphite
Graphite IGC 9390	16.1	22	Superior Graphite Co.	–	~0.338	Purified isotropic graphitic carbon. This is resilient and shows conductivity along and across the planes. Does not exfoliate when intercalated with sulfuric acid.
Graphite TIMREX MX 15	9.50–10.9	9.0	Timcal, Ltd.	>200	0.3354–0.3358	Primary synthetic graphite, high conductivity, moderate surface area.

polished samples was carried out using this X-ray detector. These X-ray maps showed the distribution of elements within the imaged surface. Because some elements can indicate certain phases (e.g. S will indicate $PbSO_4$ in a mixture of $PbSO_4$ and Pb), these were interpreted as phase distribution maps. Because detection is done with an EDS detector, the detection level of an element is on the order of 2% precluding minor or trace element mapping.

Like the SEM, the electron microprobe was used for imaging either rough or polished samples. The microprobe incorporated wavelength dispersive spectrometers (WDS) and high incident currents for X-ray detection with a lower detection limit. Two-dimensional elemental images were obtained for elements with concentrations down to about 0.5 wt% at magnifications from about 10× to 3000× with ~0.5 μm spatial resolution. In addition, stage scanning allowed large area digital X-ray, backscattered electron, and secondary electron images. We also took advantage of quantitative cathodoluminescence (CL) instrumentation which allowed the collection of light emitted during electron irradiation. For battery studies this is useful because $PbSO_4$ is a cathodoluminescent phase and a CL image rapidly shows the distribution of this phase for polished samples. The purpose of this work was to show which materials were most effective in overcoming the progressive formation of passive surface lead sulfate films during PSOC cycling.

Composite EMP images of negative plates recovered from cycled cells show a range of features. Figs. 7–10 show typical changes taking place in the negative active material composition during cycling in the absence of graphite. There are three images in each figure, marked S, Pb and CL. The S image shows the distribution of sulfur. In the color images the greater the S concentration the more yellow is the image. Lower S concentrations are characterized by a darker red coloration. The grids are very evident in these images as black rectangles (no sulfur). In the black and white images high sulfur concentrations show as light colored areas. The Pb image shows the distribution of lead which is indicated by a light grey color. The grids appear as light grey rectangles with the surrounding NAM a darker shade. The CL image shows the presence of cathodolumi-

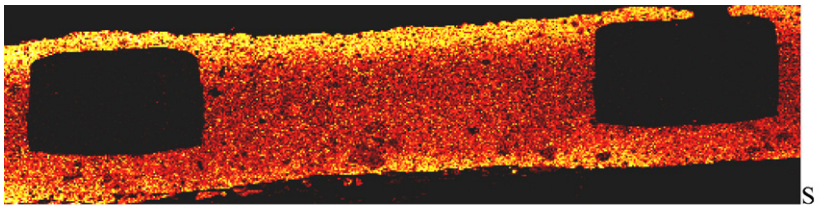

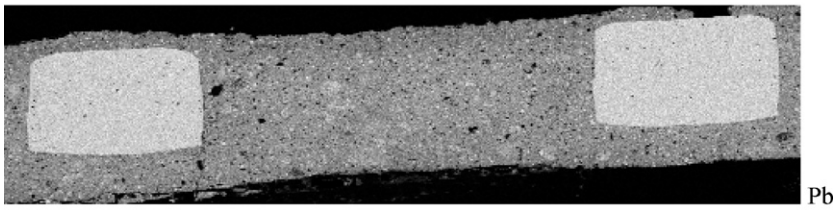

Additive composition		
	Vanisperse-A	0.6 %
	Carbon Black	2.0 %
	Graphite	0%

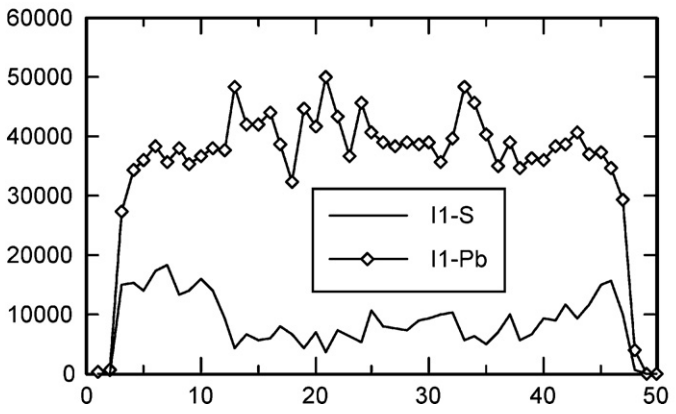

Fig. 7. Composite EMP and XRD images of negative plate cross section after formation.

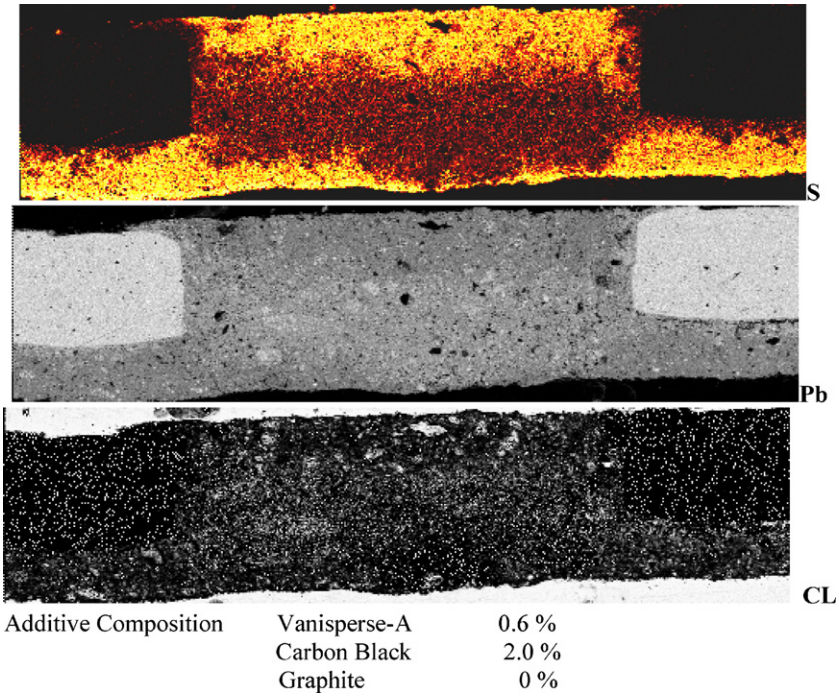

Fig. 8. Composite EMP images of negative plate cross section after 1479 PSOC cycles.

nescent phases, the most predominant being the lead sulfate since sulfur is luminescent. This is characterized by a light grey color in areas where the sulfur concentration is elevated.

The images of the formed plate (Fig. 7) show a film of lead sulfate on the surface, probably due to incomplete formation. As cycling progresses this film becomes thicker with its highest concentration at the edges of the plates. After 2139 cycles (Fig. 9) the lead sulfate zone has progressed into the interior of the plate. In contrast, Fig. 10 shows similar images of a negative plate containing 2% graphite after 3596 cycles. It can be seen that very little lead sulfate has accumulated during cycling and that this is evenly distributed through the plate. This shows that the 2939APH graphite/N134 carbon black mixture can eliminate the problem caused by buildup of lead sulfate films on the negative plate surface.

2.6. Lead sulfate nucleation studies

It is clear from the previous work that addition of graphite and mixtures of carbon black and graphite to the negative active material have the ability to suppress the formation of a lead sulfate layer on the plate surface. Consequently, a further study was carried out to determine the effect of the 2% 2939APH graphite/2% N134 carbon black mixture on lead sulfate nucleation behavior.

Additional test cells were made with negative plates containing a mixture of 2% carbon black (N134) and 2% graphite (2939APH). These were formed as previously described and then the cells were discharged to various depths of discharge as follows.

(1) Control cell with no discharge No. 2-5-6
(2) Nucleation test—10% discharge No. 2-2-6
(3) 10% discharge then recharged No. 2-2-7
(4) Nucleation test—20% discharge No. 2-3-6
(5) 20% discharge then recharged No. 2-3-7
(6) Nucleation test—40% discharge No. 2-4-6
(7) 40% discharge then recharged No. 2-4-7

The purpose of the samples in groups 1–7 was to investigate nucleation of lead sulfate in the NAM during high rate discharge and charge (2*C*) and were expected to provide demonstrable images of the distribution of lead sulfate following varying amounts of discharge/charge and then show the ability to transform the lead sulfate to lead on recharge.

2.6.1. Sample preparation procedure and data collection

Each sample was examined as a plate segment from which a sample of approximate dimensions 2 cm × 2 cm. was cut. Each sample was then embedded in epoxy to allow sampling of the active material/grid approximately normal to the plate surface. Each sample was then cut using a slow-speed saw to provide a surface sampling of four grid bars with three active material pellets between these grid bars. This surface was then ground using 600 mesh SiC paper and then polished using 9 μm and finally 1 μm diamond compound. This preparation technique has been found to minimally damage the active material and provide a reflective surface sufficient for electron microprobe analysis. Cleaning of the surface, mainly to remove oil retained after polishing, was done by immersion of the polished surface in petroleum ether, a solvent which effectively removes oil but does not affect epoxy at least in this time span. The sample was then dried at approximately 50 °C for several hours. To ensure electrical conduction, approximately 200 Å of carbon was evaporated onto the polished surface. During evaporation in vacuum, residual oil was occasionally visible on the surface; if so, the cleaning procedure was repeated.

The flat, polished and conductive samples were suitable for electron microprobe imaging. Using a CAMECA SX-50 electron microprobe, images were obtained for each of the above listed samples. Each image extended from grid bar to grid bar with image dimensions of 512 × 128 pixels. The following images were obtained simultaneously:

(1) Pb Ma—this image clearly shows the position of the grid bars and slight but clear intensity gradients in the active material due to changes in the Pb to $PbSO_4$ ratio.
(2) S Ka—this image is specific in showing the distribution of sulfates including both $PbSO_4$ and the minor $BaSO_4$.

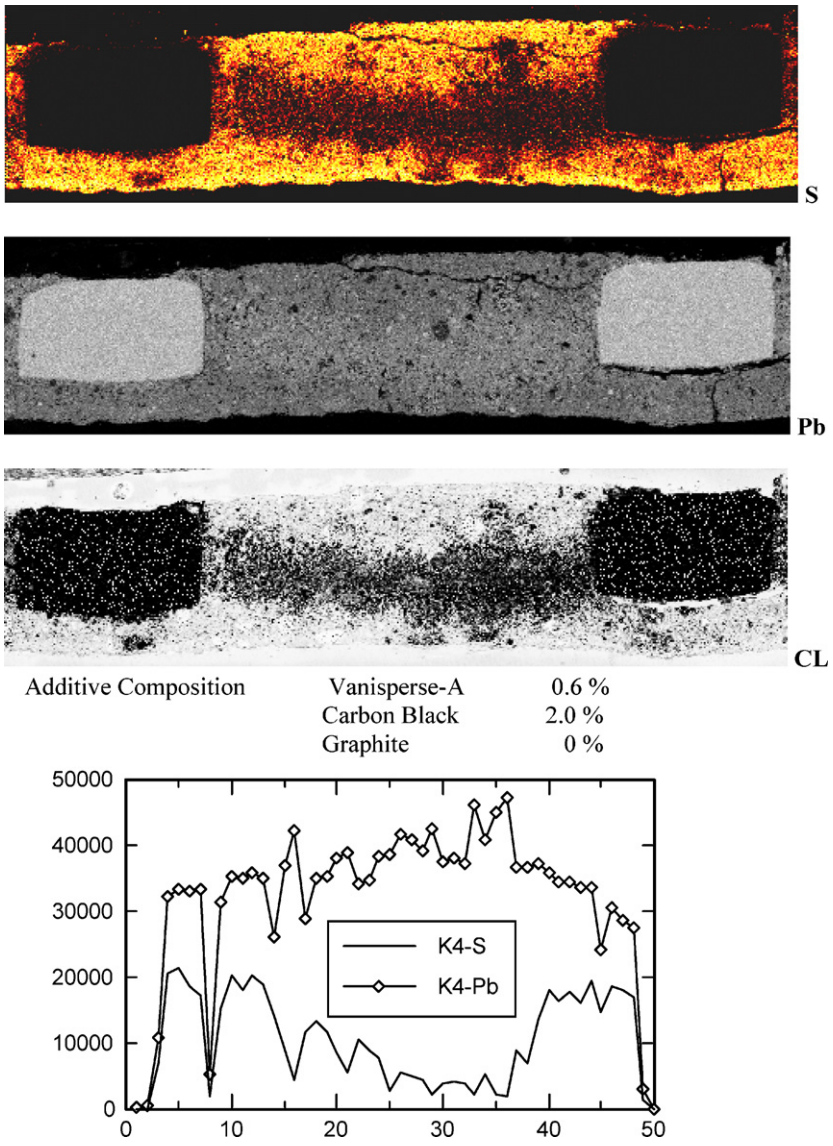

Fig. 9. Composite EMP and XRD images of negative plate cross section after 2139 PSOC cycles.

(3) Ba La—This image is specific for indicating the presence of $BaSO_4$. For coarse images, the resolution is not sufficient to resolve individual $BaSO_4$ particles with expected sizes of about 1 μm.
(4) Cathodoluminescence (CL) image—this image shows the distribution of $PbSO_4$ which is the only luminescent phase in the sample. Its contrast is usually much greater than a sulfur image.

For image collection, the accelerating voltage was set at 20 kV, and incident current of 50 nA, with a focused beam. The beam was stationary and the sample was translated at a constant rate to give an integration time of 30 ms pixel^{-1}. Each pixel represented about 10 μm but the exact value was chosen to assure coverage of the area of interest. The digital images have an 8 bit depth.

2.6.2. Results

Fig. 11 shows the data for a cell containing 2% carbon black N134 and 2% graphite 2939APH in the negative plates. Four images are shown including X-ray images for Pb, S, and Ba, as well as a CL image. The area of each image is identical. The length of these images is 512 μm × 12 μm.

The Pb image clearly shows the grid bars as the very bright rectangular areas at either end of the image with the mottled grey area between representing the active material. While not clearly resolved, there are light areas, dark areas and some texture represented in this image. These textural variations were not studied in detail since at this point we are mainly interested in the large scale features. The second image is the S distribution; however, while the active material is slightly bright, this is in fact due to normal continuum radiation giving an overall background. The grid bars also show this brightness even though no S is present. In effect this image shows no S (sulfate) present indicating that the active material is fully charged. The third image is of Ba. Again there is an overall level of brightness due to background. However, there are tiny bright specks and a careful examination shows a near 1:1 correlation of the bright pixels in the Ba image with bright pixels in the S image. This is due to BaSO4 particles. The fourth image shows the cathodoluminescence of the active material. Pb metal does not luminesce making the grid bars uniformly dark while the surrounding epoxy appears very bright. Particularly interesting in the CL image is the wealth of detail shown by various levels of brightness suggesting sub-areas (we will refer to these again later in this paper). Virtually all CL images show these effects and while not of

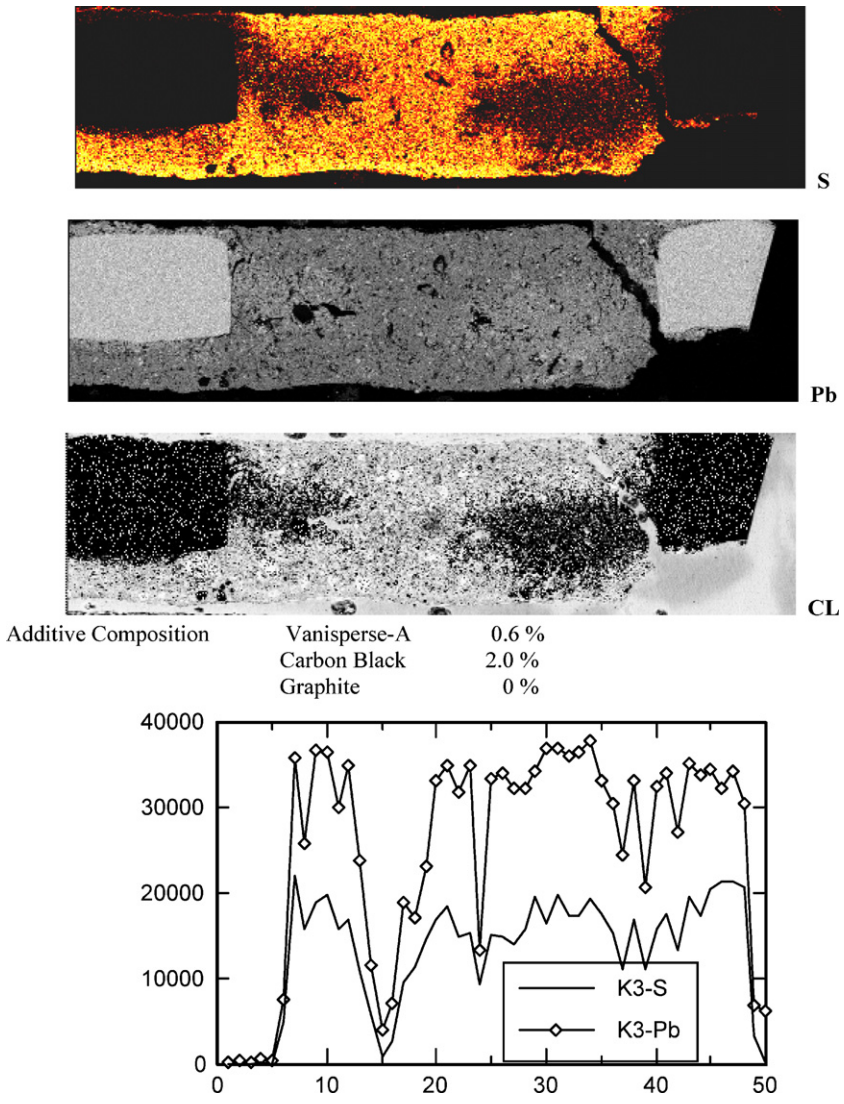

Fig. 10. Composite EMP and XRD images of negative plate cross section after 3596 PSOC cycles.

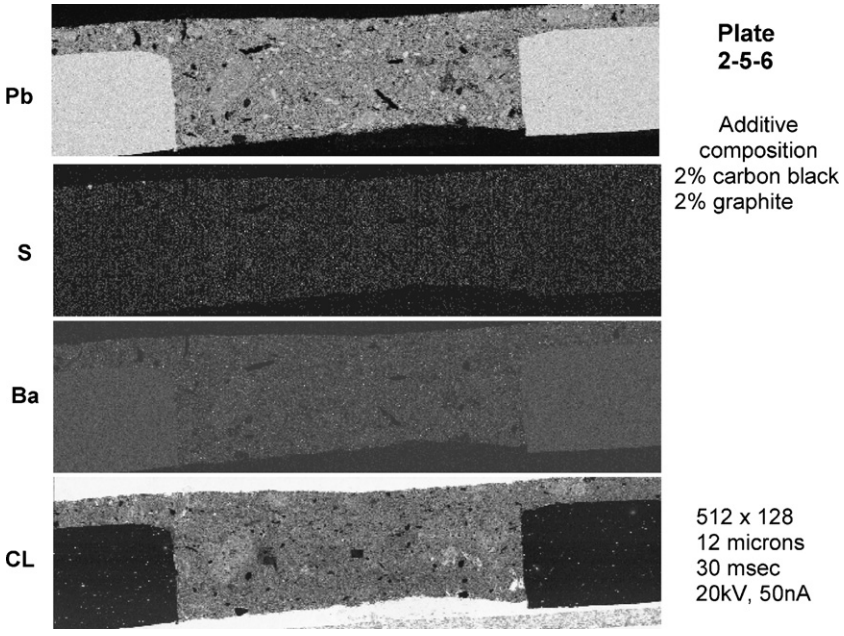

Fig. 11. Electron microprobe images of negative plate containing 2% carbon black and 2% graphite after formation.

significance here, there must be information regarding mixing, acid reactivity, homogeneity, etc in the pasted plate.

Because active material characterization may be very important, we illustrate additional information that can be obtained. Using images obtained at much higher resolution and shown below, we can use image processing to extract some textural features of the active material. Again, using sample 2-5-6, a 256 × 256 pixel image was obtained where the pixel size is 0.5 μm giving an image dimension of 128 μm on a side. In the images below (Fig. 12), we show the raw image for S and Ba, both of which show numerous bright pixels. Using standard image processing procedures, binary images were produced as shown in the center images. Careful examination shows that these images show a high correlation easily interpreted as the bright pixels representing $BaSO_4$. We thus have a direct illustration of the homogeneity and amount of $BaSO_4$ in this active material. For comparison, the rightmost image shows the Pb image where rather large Pb-metal particles are present in the active material. These lead accretions do not appear to be caused by inhomogeneity in the NAM since the Ba and S images show a homogeneous active mass.

Turning now to the samples where we are especially interested in the distribution of $PbSO_4$ in discharged and charged samples, we show below the image of Plate 2-2-6 which has been 10% discharged (Fig. 13). As before, we show the Pb, Ba, S and CL images. Again the Pb image clearly defines the components and boundaries of the plate.

Most interesting is the S image clearly showing the presence of $PbSO_4$ localized near the center of the plate and not present near the plate surface. This same distribution is shown in the CL image where the $PbSO_4$ luminesces. The discharge reaction of Pb → $PbSO_4$ has taken place near the plate center, not at the surface.

Additional information indicating the mechanism of $PbSO_4$ formation can be obtained through high resolution imaging of the active material of this same plate. Below, image processing is used to color the distribution of $BaSO_4$ (obtained from the Ba image) in comparison to the distribution of $PbSO_4$ obtained from the CL image (Fig. 14). The image at the right shows the $BaSO_4$ in blue and the $PbSO_4$ in red. Again, careful examination shows that at the center of many $PbSO_4$ grains, there is a grain of $BaSO_4$, visually confirming the nucleation of $PbSO_4$ on $BaSO_4$. The small numbers of green pixels are $BaSO_4$ particles not associated with $PbSO_4$.

Now we again turn to the partially discharged plates and show the same set of images for the sample (2-3-6) representing 20% discharge (Figs. 15 and 16). As with the 10% discharged sample, the $PbSO_4$ is entirely confined to the plate interior and is not associated with the plate boundary. This is directly illustrated in both the S and CL images below. Additional features are clearly evident in the CL

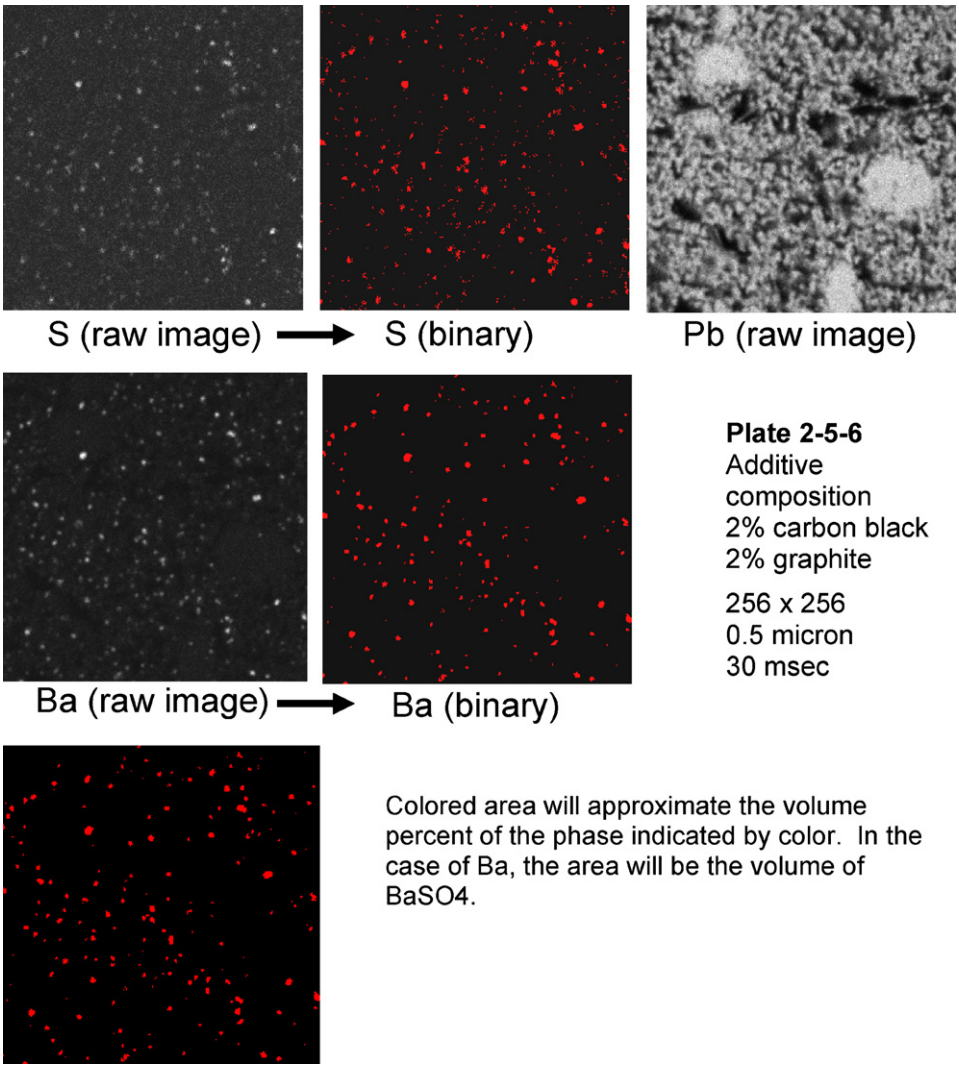

Fig. 12. Composite electron microprobe images of negative plate containing 2% carbon black and 2% graphite after formation.

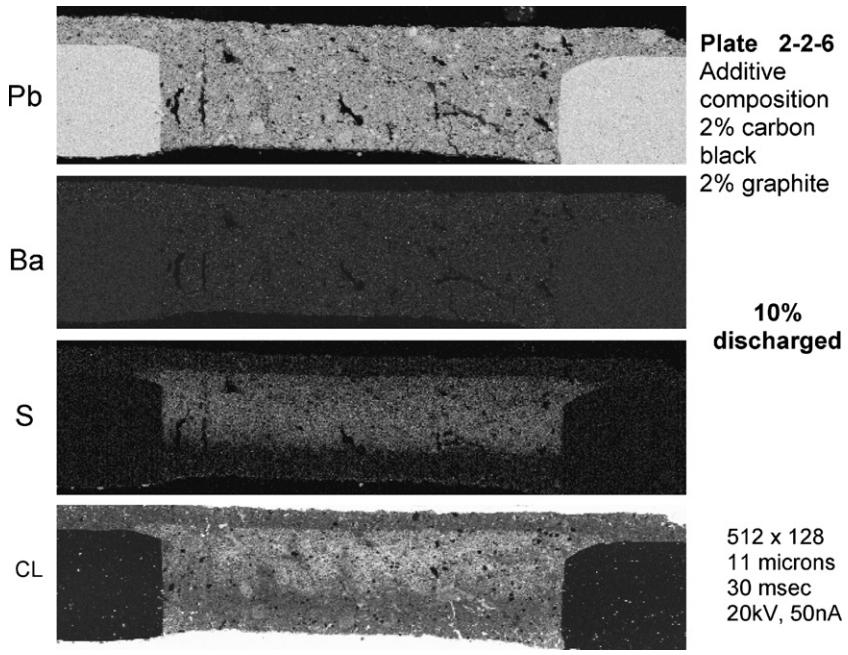

Fig. 13. Electron microprobe images of negative plate containing 2% carbon black and 2% graphite, 10% discharged.

image as discussed earlier. Here is an excellent example of how the CL variation brings out features of the active material possibly not recognizable by any other technique. For this sample, whatever causes the bright CL "stone" near the center, apparently has some effect on the $PbSO_4$ distribution where the density of sulfur in the S image is lower in the region.

At this point in the discharge there are considerably more $PbSO_4$ particles in the NAM than $BaSO_4$ particles from the expander. This suggests that once the $BaSO_4$ particles are covered with $PbSO_4$ further nucleation of $PbSO_4$ takes place on the lead grains or perhaps on the implanted carbon particles. This may have implications for expanders and suggests that higher dosage levels of $BaSO_4$ may be beneficial.

The following and last set of images (Figs. 17 and 18) show the sample (2-4-6) discharged to 40%. The trend continues where the formation of PbSO4 clearly is confined to the plate interior, and not at the plate surface and is rather uniformly distributed. This is again shown by both the S image and the CL image.

While not shown, the images of the recharged plates (2-2-7, 2-3-7, and 2-4-7) show no residual PbSO4 indicating that all the PbSO4 can be converted back to lead. Where previous studies of negative plates in the PSOC mode have demonstrated the formation of PbSO4

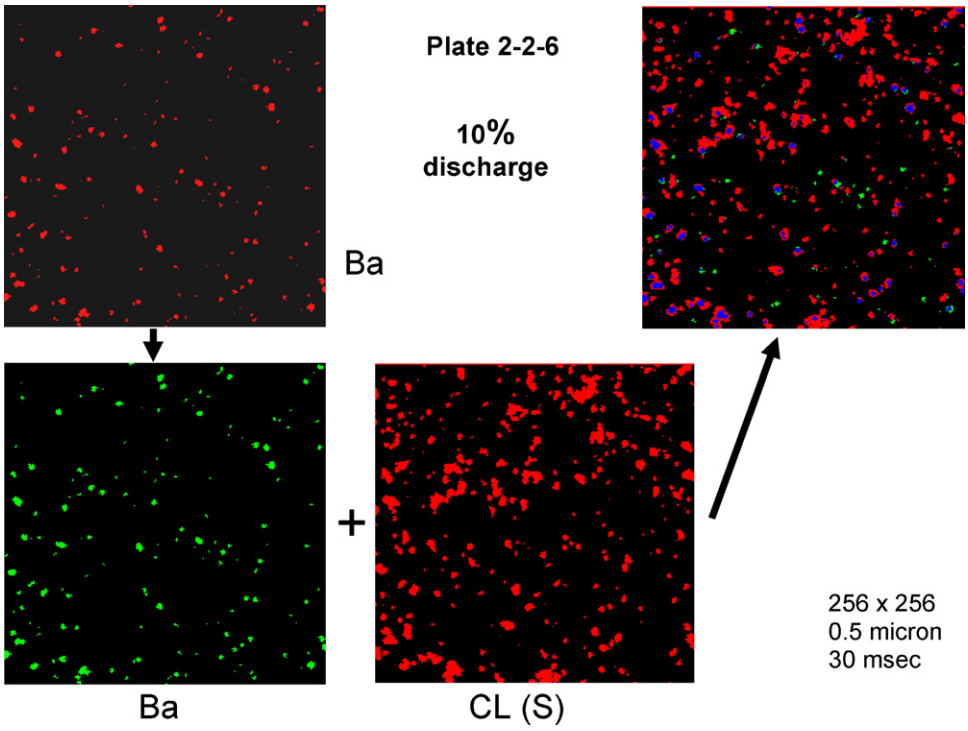

Fig. 14. Composite electron microprobe images of negative plate containing 2% carbon black and 2% graphite, 10% discharged.

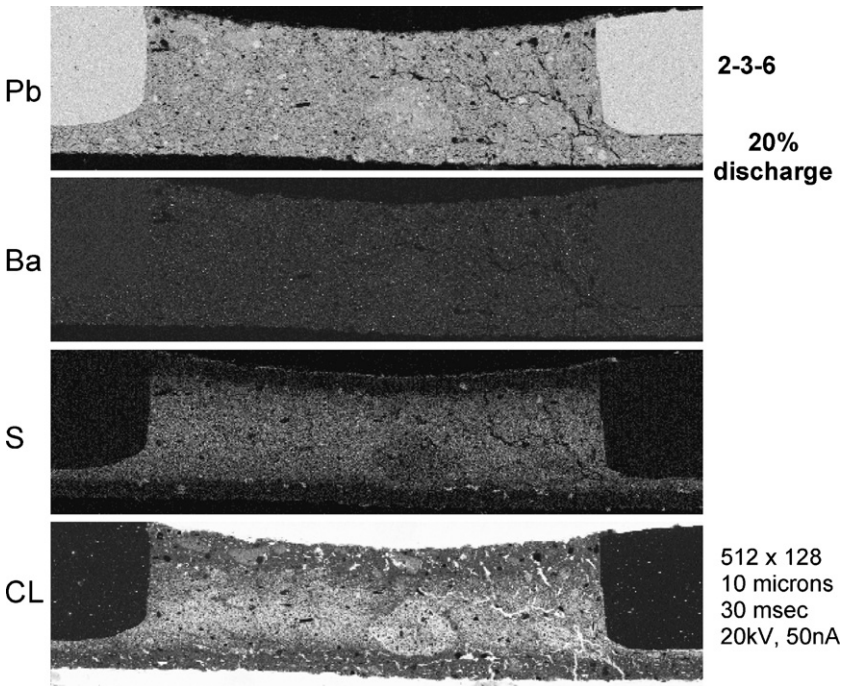

Fig. 15. Electron microprobe images of negative plate containing 2% carbon black and 2% graphite, 20% discharged.

at the surface that cannot be converted back to lead on recharge, the sequence of our test results show that this effect has been reduced, if not completely eliminated, by the carbon additives.

At this point we have shown that carbon additives to the NAM increase its cycle life under PSOC conditions. Furthermore, the additives are effective in changing the distribution of $PbSO_4$ in the discharged NAM from the surface to the interior.

2.6.3. Work program—task two

The previous work, while demonstrating improvements to PSOC cycle life from addition of graphite/carbon black mixtures, does not give any indication, from the many types available, of which types of carbon black and graphite are optimum. Nor does it allow prediction of how properties of various types of carbon influence the life of VRLA batteries in PSOC operation. We therefore designed an experiment where a wider range of carbon materials was tested including four different types of graphite, four activated carbons and two types of carbon black. These were chosen to have a wide range of properties in an attempt to correlate these properties with PSOC life. The concentrations of Vanisperse A and barium sulfate were held constant at 0.2% and 0.8% respectively. The relevant physical properties of these materials are shown in Tables 6–8.

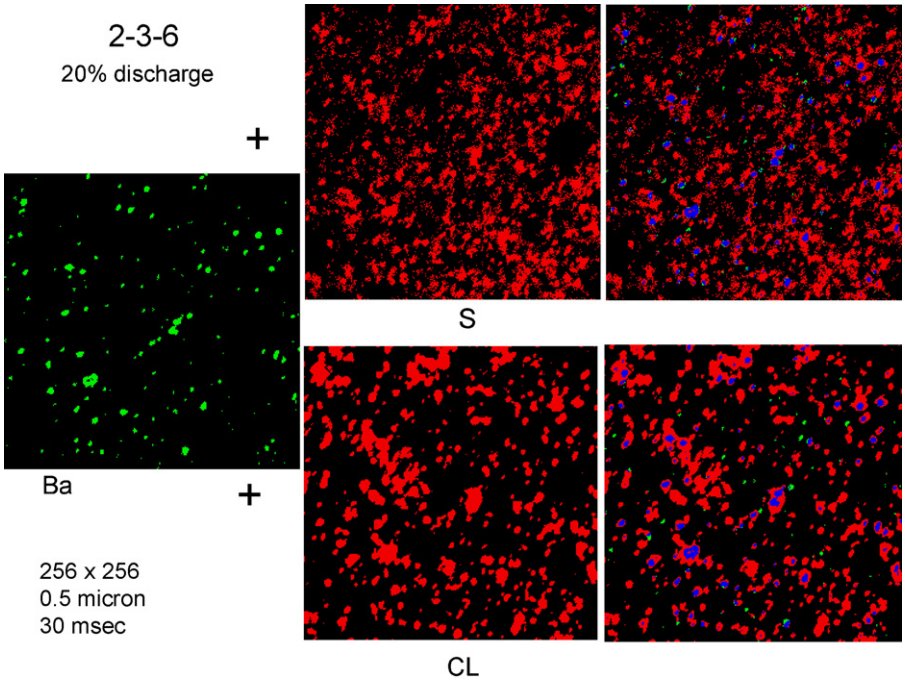

Fig. 16. Composite electron microprobe images of negative plate containing 2% carbon black and 2% graphite, 20% discharged.

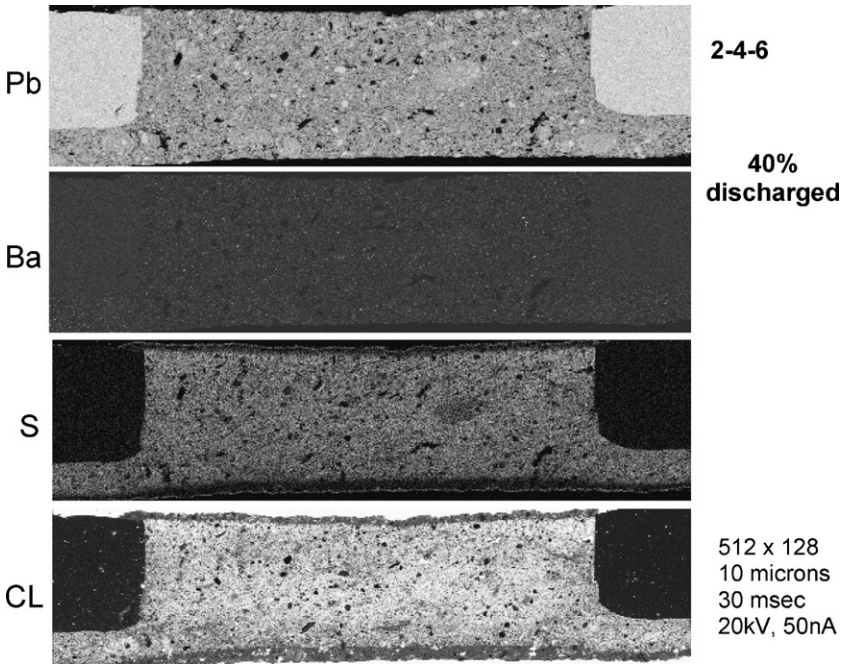

Fig. 17. Electron microprobe image of negative plate containing 2% carbon black and 2% graphite, 40% discharged.

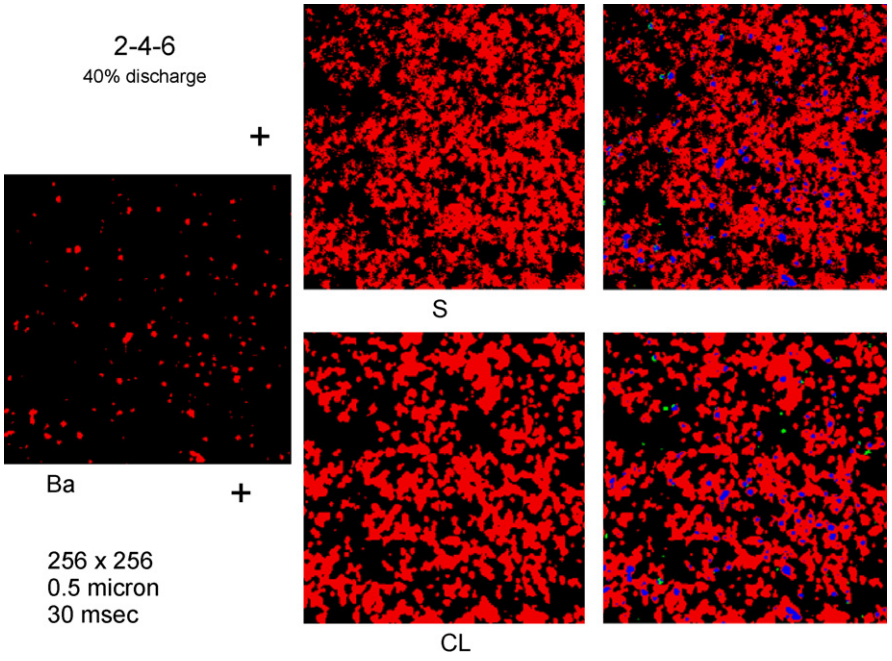

Fig. 18. Composite electron microprobe images of negative plate containing 2% carbon black + 2% graphite, 40% discharged.

Table 7
Properties of carbon black materials used in Task 2.

Additive	BET specific surface area ($m^2\ g^{-1}$)	Mean particle size, D_{50} (nm)	Supplier	Description
Carbon Black N134	143	18	S.D. Richardson Carbon Co.	Carbon black with moderate surface area, high structure and small particle size. Conductivity $100\ \Omega^{-1}\ cm^{-1}$
Carbon Black Soltex Ace Black	75	20	Soltex Synthetic Oils and Lubricants, Inc.	High purity carbon black, derived from acetylene (also known as Acetylene Black).

Table 8
Properties of MeadWestvaco activated carbons used in Task 2.

Additive	BET specific surface area ($m^2\,g^{-1}$)	Mean particle size, D_{50} (μm)	Micro to total pore volume ratio	Description
Activated Carbon MWV-A	1780	39.5	0.36	Low micro porosity carbon, low impurity
Activated Carbon MWV-B	2357	39.0	0.46	High Porosity carbon, low impurity
Activated Carbon MWV-C	1683	33.4	0.37	Low micro porosity carbon, low impurity
Activated Carbon MWV-D	1126	23.7	0.90	High micro porosity carbon, low impurity

2.7. Graphites

The four graphite types have very different crystalline, textural and physical properties. They belong to four separate families of graphitic carbon: natural flake graphite, expanded graphite, isotropically graphitized carbon (IGC) and synthetic graphite.

Specific surface areas range from 9 to 24 $m^2\,g^{-1}$, D_{50} particle sizes are similar (9 μm) with the exception of IGC9390 (22 μm).

2.8. Carbon blacks

Two carbon black types were selected for this study, N134 as used in Task 1 and Ace Black, a high purity acetylene black. Previous work with carbon black has been reported elsewhere [1,4].

2.9. Activated carbons

The four activated carbon materials were supplied by the MeadWestvaco Corporation. These exhibit very high specific surface areas, median particle sizes between ~23.7 and ~39.5 μm, and present mid to high micropore/total pore volume ratios. Following the (IUPAC) recommendation we define micropores as having width <2 nm, mesopores having widths between 2 and 50 nm, and macropores with widths exceeding 50 nm. Considering the radius of the SO_4^{2-} (0.149 nm) and Pb^{2+} (0.119–0.146 nm) ions, it appears that these species may be able to enter the micropores (if hydration spheres are neglected).

2.10. Resistivity of lead sulfate and carbon mixtures

To simulate the effect of the additives on the resistivity of discharged NAM samples of the additives in a pure lead sulfate matrix were prepared by weighing out 0.5, 1.0, 1.5, 2.0, 3.0, 4.0 g of the individual raw materials, or 0.25, 0.5, 0.75, 1.0, 1.5, 2.0 g of each in the case of 2 component mixtures. Pure dry lead sulfate powder (American Elements, >99% purity and $D_{50} \sim 5.6$ μm) was then added to each sample to make up the total weight to 100 g.

The individual mixtures were milled in a cylindrical plastic drum (diameter 12.5 cm, height 12 cm, volume approximately 0.15 l) using a geological rock tumbler. Ceramic milling media were used in preference to steel balls to avoid the introduction of conductive metallic impurities. The total milling time for each sample was 30 min to ensure a homogeneous mixture. The resulting range of mixtures had weight percent concentrations of 0.5, 1.0, 1.5, 2.0, 2.5, 3.0 and 4.0. The powdered sample was compressed at a fixed pressure of 1655 bars to remove voids and produce a pellet. The pellet was then placed in a Teflon cylinder between a fixed circular base plate and piston (both stainless steel) and compressed at 117 bar. The resistance was measured across a Wheatstone bridge using a Keithly 6517A multimeter for high resistances and a Tektronix TX3 for low resistances. The volume resistivity (ρ) in Ω cm was calculated from:

$$\rho = R\left(\frac{S_0}{d}\right)$$

where S_0 is the apparent surface area, d is the compressed sample thickness and R is the measured resistance.

Plots of resistivity versus additive concentration allow us to demonstrate the presence or absence of a conductive percolation point for the additive of interest, i.e. the concentration above which the composition becomes conductive. Plots of resistivity versus concentration for the graphite, carbon black and activated carbon types are shown in Figs. 19–21. Also shown are the resitivity values of a 2% dosing of the additive in dry, unformed NAM. The graphites, 2939APH, IGC 9390 and MX15 show a percolation point between 2.5% and 3.0% dosing. The expanded graphite, ABG1010, produces

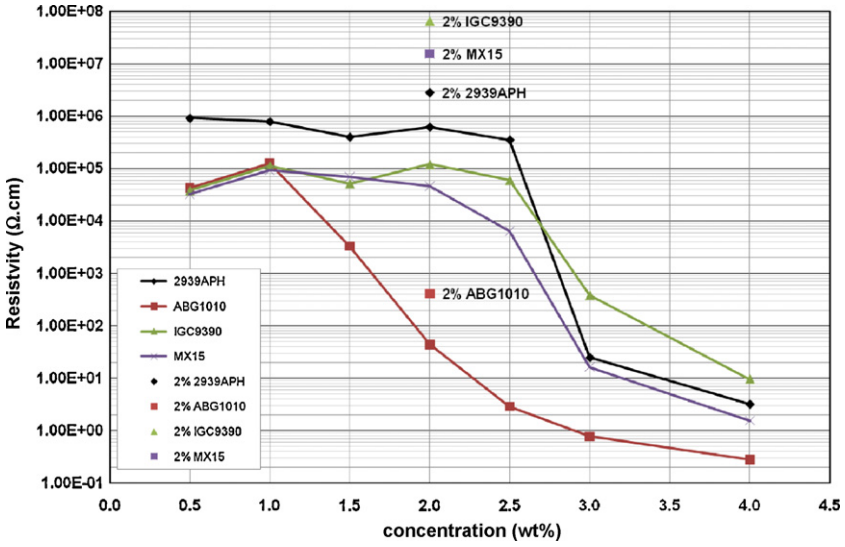

Fig. 19. Resistivity of graphite materials in lead sulfate and at 2% loading in dry, unformed active material.

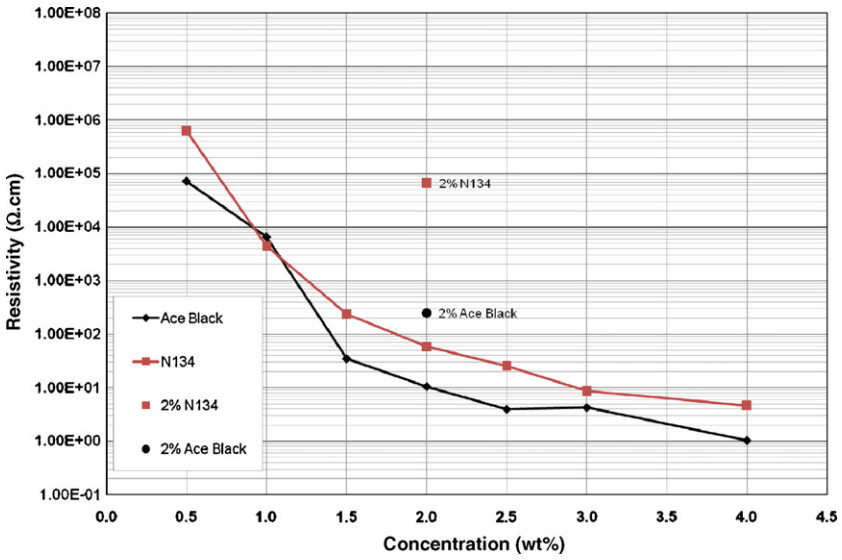

Fig. 20. Resistivity of carbon blacks in lead sulfate and at 2% dry loading in dry, unformed active material.

lower resistivity with a progressive reduction between 1% and 3%. The carbon blacks show a gradual reduction in resistivity with concentration (Fig. 20) with macro conductivity becoming evident at a 1.5% dosing level. As shown in Fig. 21 the activated carbons have no effect on the resistivity of lead sulfate over the concentration range studied. The higher conductivity of carbon black-containing mixtures probably reflects (a) that the carbon particles are very small and can easily fit between the sulfate grains and (b) the number of particles per gram is very large.

Since the conductive behavior of carbons is largely attributable to the degree of sp^2:sp^3 hybridization it follows that the more amorphous carbons are generally poorer conductors, but particle density and size also play an important role. For example, if the particle count per unit volume is very high, as in the case of carbon black, then the inter-particle spacing is low and may give rise to conductivity via electron tunneling.

Steric factors also may play a role in the degree of observed resistivity. The basal plane of flake graphite may prove relatively inert, whilst the edges of flakes expose a much more varied electrostatic topography with much greater chemical activity.

2.11. Resistivity of dry unformed negative active material

The experimental matrix is shown in Table 9. Negative plates were produced from these mixtures as previously described. After curing, the material was detached from the lead grid, ground and sieved (100 mesh). The resistivity was then measured as before. The dry unformed material from pasted plates is a complex mixture containing basic lead sulfates, lead oxide, barium sulfate, lignosulfonate, etc. The values determined for the unformed plate material are plotted in Fig. 22.

As expected, the resistivity of the cured plates was high for all that contained activated carbons. In the case of the plates that contained graphite, carbon black and mixtures of these materials the data are more complex but show lowered resistivity with values depending on the composition of the additive. It should be recalled, from the resistivities of the lead sulfate/additive mixtures, that at these dosage levels only ABG1010 graphite and the two carbon blacks had any significant effect on resistivity. Therefore the present result is not surprising since all the other mixtures containing graphite are below their percolation point concentrations. This suggests that, if resistivity is an important factor in PSOC cycle

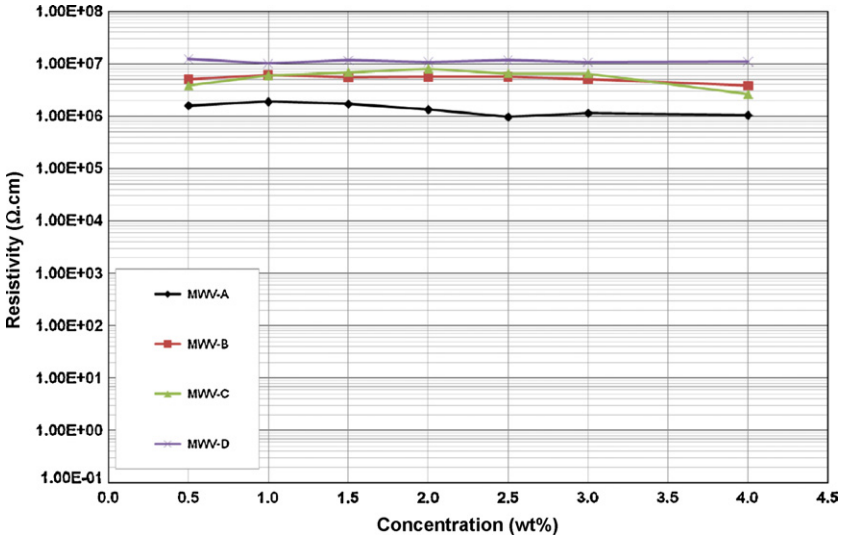

Fig. 21. Resistivity of activated carbons in lead sulfate.

Table 9
Experimental groups and additive dosing levels for Task 2 studies.

Sample no.	Mixture composition	Wt% dosing in NAM
1	2939APH	2%
2	2939APH + MWV A	1%:1%
3	2939APH + MWV B	1%:1%
4	2939APH + MWV C	1%:1%
5	2939APH + MWV D	1%:1%
6	2939APH + N134	1%:1%
7	2939APH + Ace Black	1%:1%
8	N134	2%
9	Soltex Ace Black	2%
10	ABG1010	2%
11	ABG 1010 + MWV A	1%:1%
12	ABG 1010 + MWV B	1%:1%
13	ABG 1010 + MWV C	1%:1%
14	ABG 1010 + MWV D	1%:1%
15	ABG 1010 + N134	1%:1%
16	ABG 1010 + Ace Black	1%:1%
17	IGC9390	2%
18	IGC 9390 + MWV A	1%:1%
19	IGC 9390 + MWV B	1%:1%
20	IGC 9390 + MWV C	1%:1%
21	IGC 9390 + MWV D	1%:1%
22	IGC 9390 + N134	1%:1%
23	IGC 9390 + Ace Black	1%:1%
24	MX15	2%
25	MX 15 + MWV A	1%:1%
26	MX 15 + MWV B	1%:1%
27	MX 15 + MWV C	1%:1%
28	MX 15 + MWV D	1%:1%
29	MX 15 + N134	1%:1%
30	MX 15 + Ace Black	1%:1%
31	MWV-A	1%
32	MWV-B	1%
33	MWV-C	1%
34	MWV-D	1%

life, we should obtain the best results from cells with plates containing 2% Ace black and 2% ABG1010 graphite. It also suggests that in future work 2939APH, IGC9390 and MX15 graphite should be used at concentrations greater than 2.5%.

2.12. Experimental design for electrochemical testing

To test the effect of the additives in electrochemical cells, the materials of interest were incorporated into negative plates as previously described. The experiment was been designed as a partial matrix, so that each of the individual raw material components was added separately at one concentration (2%, 10 variables), and, additionally, each graphite was combined with either, an activated carbon, or a carbon black at concentrations of 1% each (24 Variables). The experimental design is shown in Table 10.

The dosing levels in this part of the project were fixed to limit the number of experimental variables where the total additive concentration is ~2 wt% with respect to the lead oxide quantity, with the exception of the activated carbons where 1 wt% was used, based on the supplier's recommendation.

2.13. Electrical testing

2.13.1. Initial capacity

Four cells for each additive were assembled, filled and formed as previously described. On completion of formation each cell was cycled 10 times at the nominal C-rate (1.74 Ah was used as in previous work to aid comparison of capacity data). The 1st and 10th discharge capacities were obtained to ensure complete formation as shown in Fig. 23. The data represent the average capacities from 4 cells. Capacity increases were observed for all cells from cycle 1 to cycle 10, as expected, reflecting further formation of the active material and establishment of an equilibrium acid saturation in the plates and separators. The capacities within individual groups were quite reproducible, while the capacity differences between groups were far more pronounced. Notably, the control cells gave very similar capacities, but were generally lower with a smaller increase with cycling. The greater increase in capacity with cycling in the cells with higher carbon loadings suggests that carbon has an inhibiting effect on formation charge acceptance. The observed variability between the test groups reflects not only the additive performance but also porosity, density and saturation effects. The much higher capacities evidenced by some carbon containing cells is of great interest and indicates increased active material utilization.

The cells containing flake graphite 2939APH, either alone or in mixtures with carbon black or activated carbon, gave the greatest first cycle capacities (first cycle capacity >65 mAh g^{-1}) and these also show a significant gain in capacity with cycling (all 2939APH cells gave tenth cycle capacity >80 mAh g^{-1}). Overall the greatest gain in capacity is seen for the cells containing Ace Black, N134

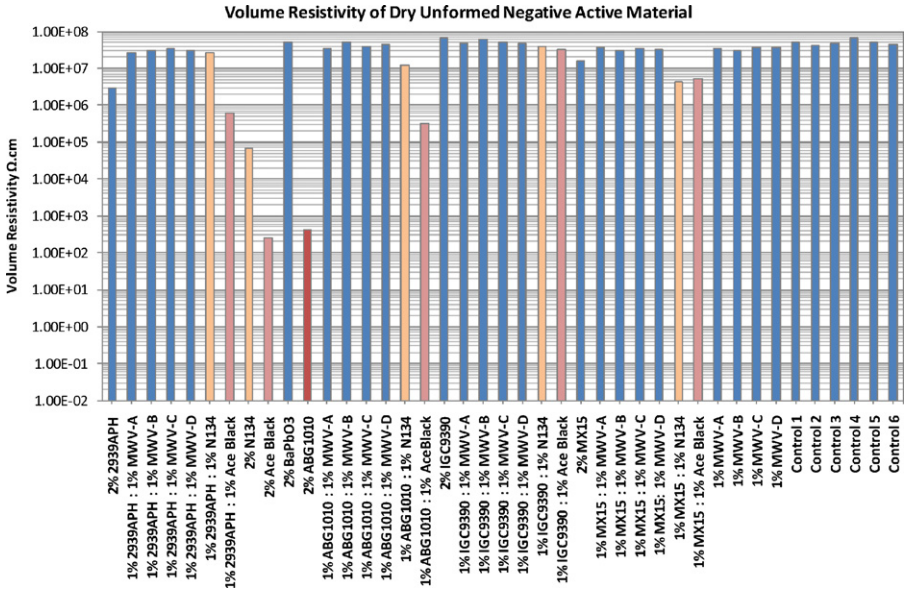

Fig. 22. Resistivity measurements for dry, unformed active material samples.

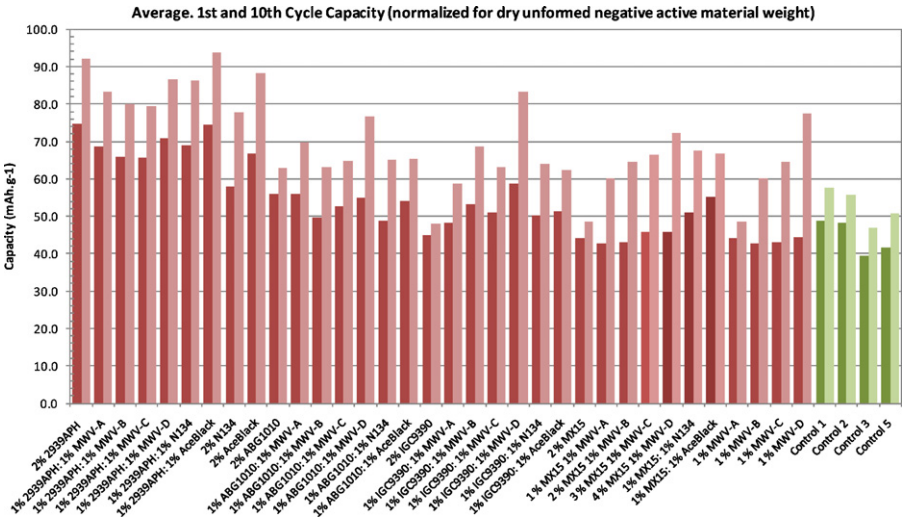

Fig. 23. First and tenth cycle capacities (average of of 4 cells) from each group normalized for unformed negative active material weight.

and MWV-D. This result confirms the findings of Task 1. For the mixtures containing activated carbon MWV-D, the capacities are consistently greater than the other activated carbons. The controls and the cells with isotropically graphitized carbon give the lowest capacities.

The large capacity gains seen for NAM containing high carbon levels may indicate that the carbon is acting in the same way as a traditional battery expander by increasing the sponge lead surface area and acting as a nucleating agent. This 'expander action' may be responsible for the 1st to 10th cycle capacity increases seen for the two carbon blacks. These have very fine particles hence the number of nucleation sites is much higher.

The other notable capacity increase is seen for all plates containing MWV-D, an activated carbon from organic material.

2.13.2. PSOC cycling

The cells from each group were placed on the PSOC cycling test. The cycling profile was modified from that used previously by setting the charge and discharge currents slightly higher at 5 A (2.8*C*-rate).

Fig. 24 shows the PSOC cycling data from the best performing additives compared to the control cells. The data for each additive is displayed as a series of bars where each bar represents the number of cycles obtained in a cycle set. The number of cycles obtained in a cycle set is a measure of the charge acceptance of the additive during the 2.8*C* rapid cycling. It can be seen that the number of cycles obtained during a cycle set reduces as the number of cycle sets increases. This shows that the high-rate charge acceptance declines with cycling. However, the loss in capacity can be recovered by charging showing the ability of the additives to aid recharge of lead sulfate that has accumulated in the plate as a result of reduced charge acceptance. Fig. 25 shows the capacity at the end of each cycle set following a charge at 4.0 A for 5 h with a cell voltage limit of 2.45 V.

Table 10 shows the number of cycles for each group. Several of the groups have achieved over 150,000 cycles and up to 27 cycle sets.

At the time of preparing this paper all of the cells are still cycling, therefore it is not possible to select an additive that is unequivocally superior. Because of practical issues, such as circuit availability, cycling of some test groups began later than others therefore they have accumulated fewer total cycles.

Impressive cycling behavior has been shown by many of the additives. Of the graphite materials, 2939APH has given the best result so far and excellent performance has also been obtained from mixtures of 1% 2939APH and carbon black. Cells with 2% Ace Black also performed very well. Care needs to be taken in interpreting these data since the cells are still undergoing cycling and may be capable of many more cycles. However, it is clear that additives containing graphite and carbon black give excellent cycle life.

Further understanding of the role of the carbon additives on PSOC cycling behavior can be gained from the relationship between the cell voltage at the end of charge and the end of discharge during the rapid cycling routine at 50% DOD. Fig. 26 shows the behavior of cells containing 0.1% and 2% Ace Black in the negative electrodes. With the lower carbon loading, similar to that used in conventional batteries, the cell voltage rises rapidly, following the start of the rapid cycling, to 2.7 V. When the carbon loading is increased to 2% this initial voltage increase is eliminated indicting that the greater amount of carbon has a significant effect on the charge kinetics. The polarization is significantly reduced showing that the charge process has become more reversible. In the case of the end of discharge voltages, polarization is also reduced resulting in an increased number of cycles before the termination voltage is reached.

The effect of adding carbon black can also be seen in Fig. 27 which shows the behavior of cells containing 2% 2939APH graphite and a mixture of 1% 2939APH and N-134 carbon black. When the graphite is used alone the cell voltage increases to 2.8 V shortly

Table 10
High rate PSOC cycling summary showing total cycles and cycle sets (in parentheses).

	No second component	MWV-A	MWV-B	MWV-C	MWV-D	N134	Ace Black
No second component	Controls: 139,643 (27)	96,848 (13)	96,851 (12)	88,494 (12)	117,916 (15)	139,738 (27)	150,588 (21)
2939APH	155,117 (19)	151,147 (20)	140,618 (26)	147,377 (21)	144,345 (19)	150,062 (18)	116,350 (17)
ABG1010	139,967 (31)	140,627 (28)	148,316 (28)	138,737 (26)	152,599 (22)	146,992 (24)	136,758 (25)
IGC9390	126,521 (32)	145,740 (22)	144,558 (21)	149,334 (28)	58,931 (10)	137,525 (24)	144,074 (26)
MX15	101,969 (19)	88,499 (12)	88,452 (11)	95,559 (14)	89,324 (12)	145,816 (24)	147,013 (26)

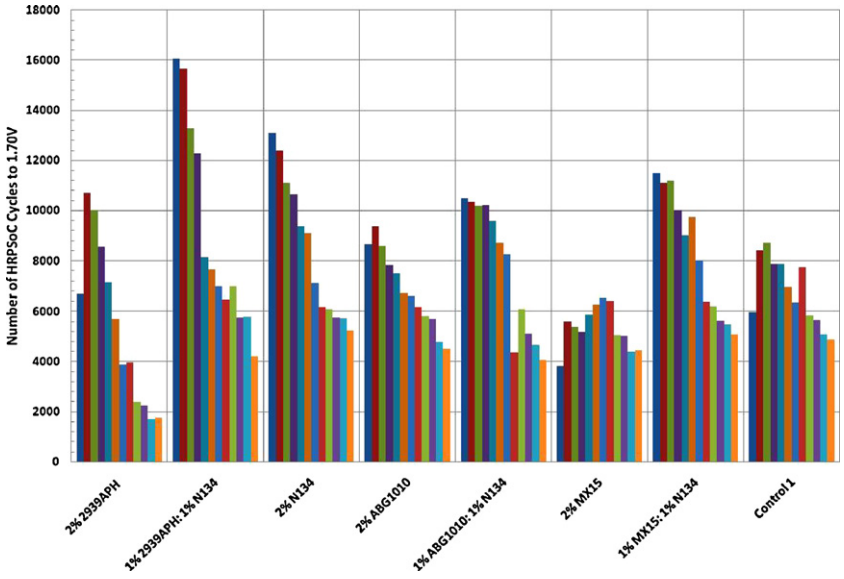

Fig. 24. PSOC cycling data from cells with the best performing additives compared with the control cells.

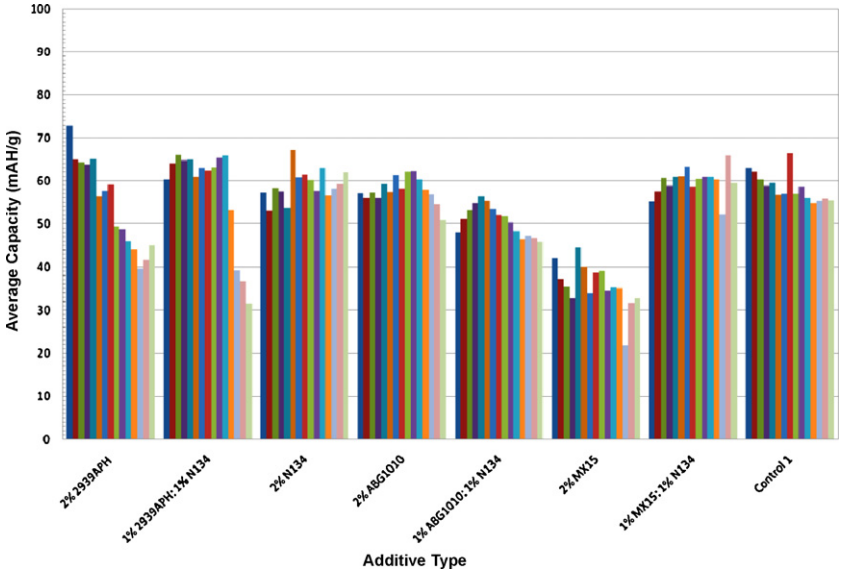

Fig. 25. Capacity of cells after recovery charging following PSOC cycling. Each bar represents a cycle set.

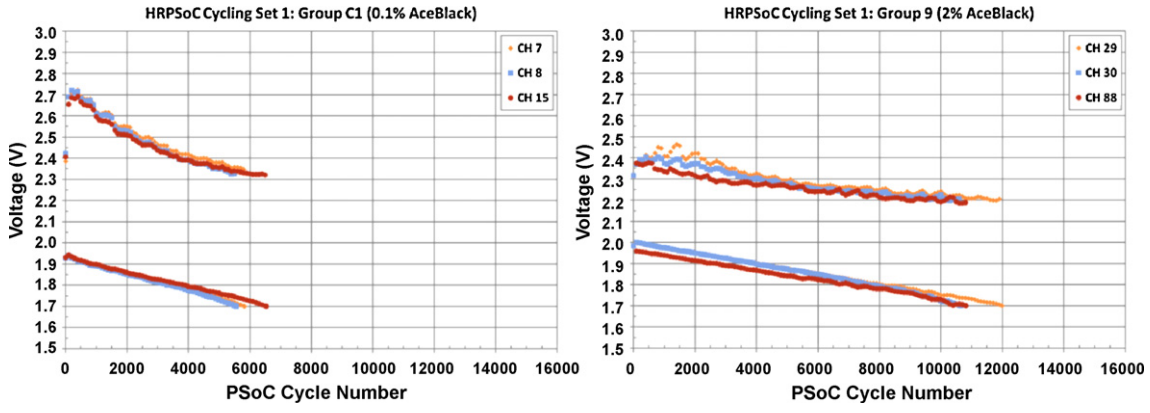

Fig. 26. Examples of end of charge and end of discharge cell voltages during PSOC cycling. Cells containing Ace Black.

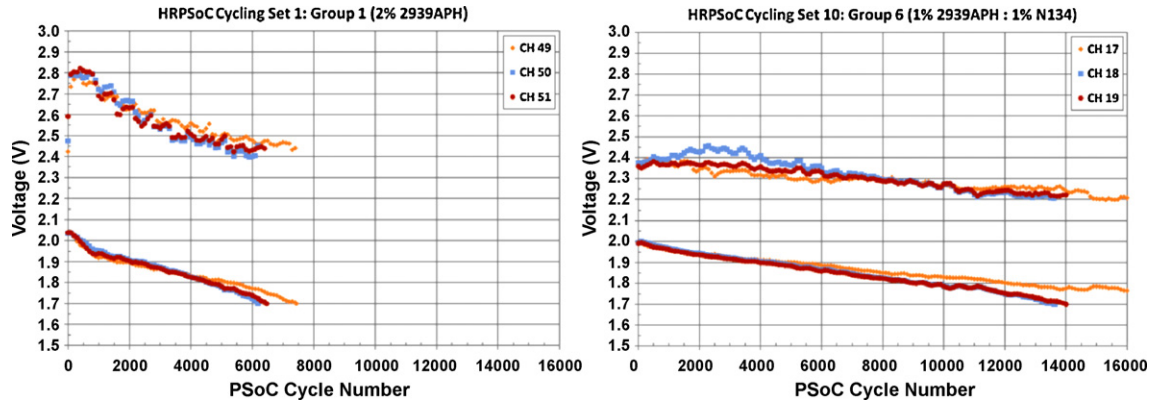

Fig. 27. Examples of end of charge and end of discharge cell voltages during PSOC cycling. Cells containing 2939APH and N-134 carbon black.

after cycling is started. When the graphite is mixed with carbon black the voltage increase is suppressed. This is an important phenomenon in the context of electric vehicle batteries that receive some of their charge from regenerative braking. At 2.8 V per cell regenerative braking would be ineffective and the battery would not receive charge. Again, the effect on the discharge behavior can also be seen. A greater number of cycles is obtained before the cell voltage drops to the cut-off value of 1.7 V per cell. The mixture of 1% 2939APH graphite and N-134 carbon gives excellent cycle life and charge acceptance. The activated carbons form a much broader shoulder as seen in Fig. 28 although that for MWV-D is less pronounced. The end of charge voltages are higher than those of the 2939APH + N-134 carbon black mixtures.

2.14. Changes to plate morphology during cycling

One cell from each group was torn down to examine the fully formed negative plate condition before PSOC cycling. Plates were extracted from the cell groups, washed in running water for 12 h, then dried in an oven at 110 °C.

Figs. 29–31 are examples of typical crystal morphologies of negative plates before cycling and after 100,000 cycles showing changes that take place with cycling. It is clear that the morphology of the formed NAM before cycling is not changed appreciably with the choice of additive. The three examples shown all have similar characteristics and are generally typical of formed NAM. The lead metal is present as a network of linked grains forming a

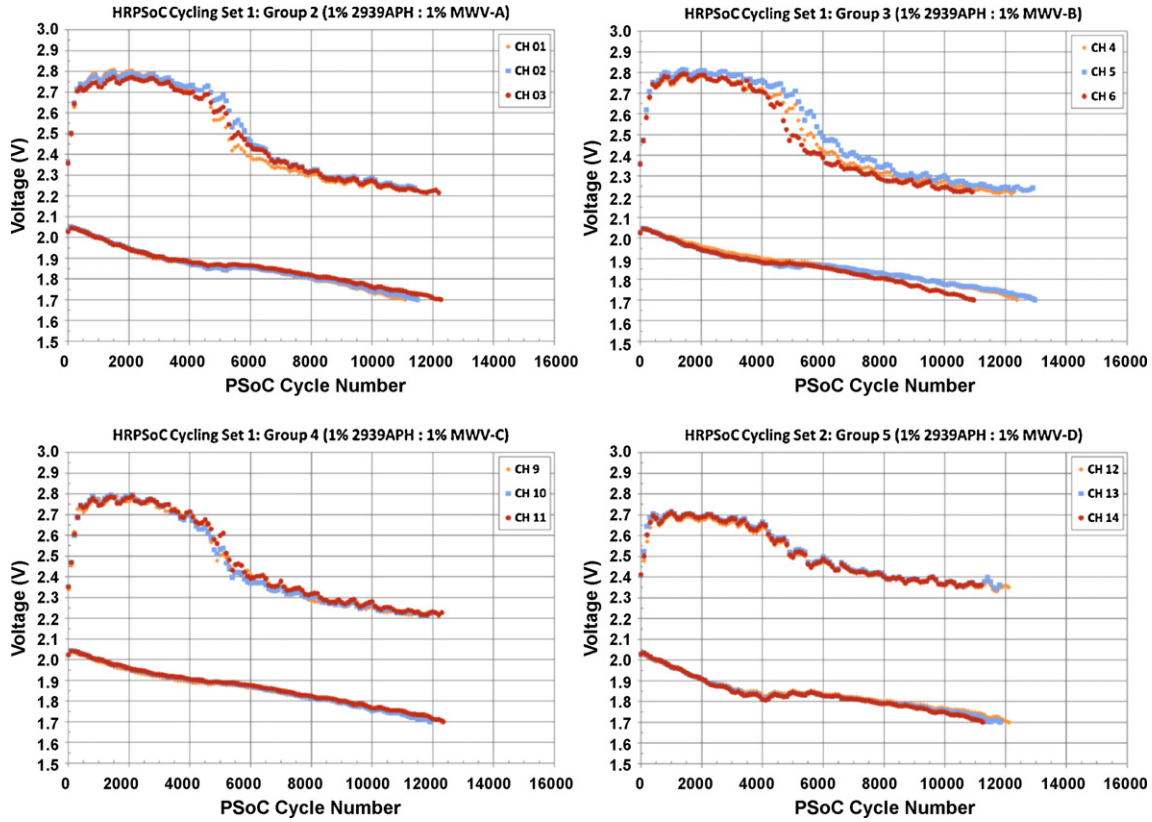

Fig. 28. Examples of end of charge and end of discharge cell voltages during PSOC cycling. Cells containing 2939APH and MWV-A, MWV-B, MWV-C and MWV-D activated carbon.

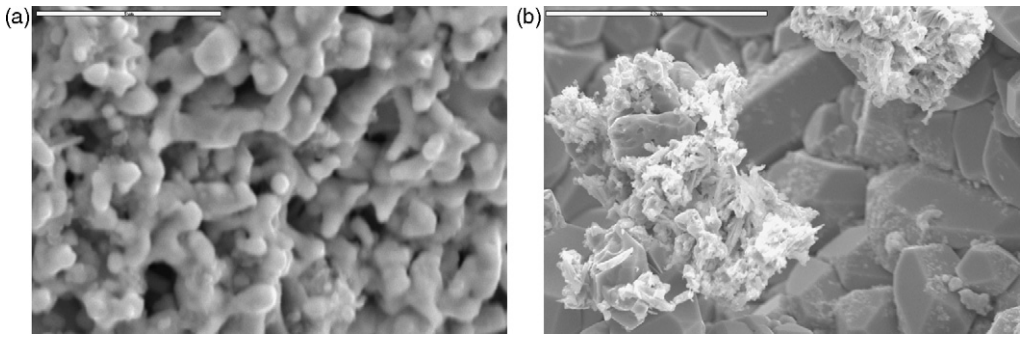

Fig. 29. Comparison of crystal morphologies of standard charged negative plates after formation (left) and after 100,000 PSOC cycles (right). Scale bars 5 and 20 μm respectively.

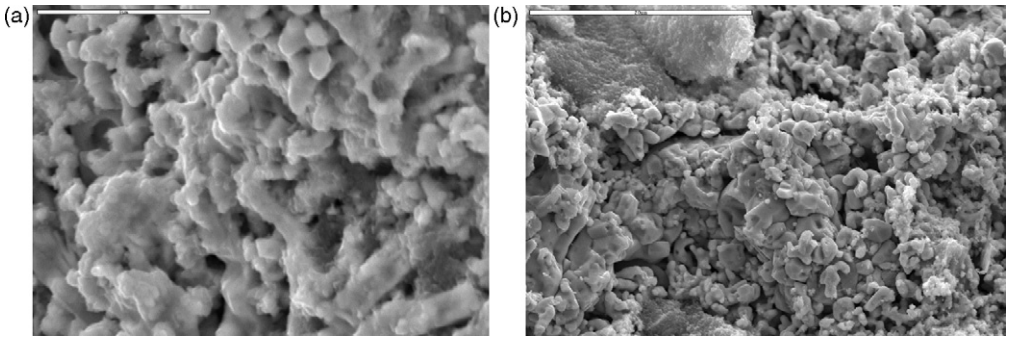

Fig. 30. Comparison of crystal morphologies of charged negative plates with 1% 2939APH graphite plus 1% N134 carbon black after formation and after 100,000 PSOC cycles. Scale bars 5 and 20 μm respectively.

continuous structure. The effect of the additives on the structure after 100,000 PSOC cycles is quite pronounced. In the case of the standard plate with 0.1% carbon loading a large concentration of lead sulfate crystals is clearly visible in the cycled plate. The plate containing a mixture of graphite and carbon black has virtually no lead sulfate in the NAM. However, when activated carbon is substituted for carbon black a large amount of lead sulfate is again evident. This correlates well with the cycle life data which shows the longest life from plates containing both graphite and carbon black. This is the case whether the graphite is of the flake, expanded or synthetic variety, or whether the carbon is oil-based or acetylene based. None of the test mixtures with activated carbon gave long life.

BET surface area measurements (Table 11) show that the specific surface areas of the active mass are decreasing with cycling, with the significant exception of 1% 2939APH with 1% N134, which continues to increase.

2.15. Electron microprobe and cathodoluminescence images

Plates from the best performing additive mixtures at 50,000 cycles were examined by a scanning electron microprobe (EMP). This technique allows us to look for differences between areas in the active material. Given the excellent performance from mixtures of 2939APH graphite with carbon blacks these plates were selected for examination.

The EMP scans show a very interesting feature where carbon flakes (graphite) are visible at the center of areas of lead metal. Surrounding these areas we find lead sulfate. It would appear that the lead is deposited on or near to the graphite flakes, probably during charge when Pb^{2+} ions in solution capture electrons stored on the graphite and deposit as lead metal. This probably explains the reduction in BET surface area with cycling since the high surface area carbon is becoming buried under a lead metal deposit. Figs. 32–33 show cross sections of a plate con-

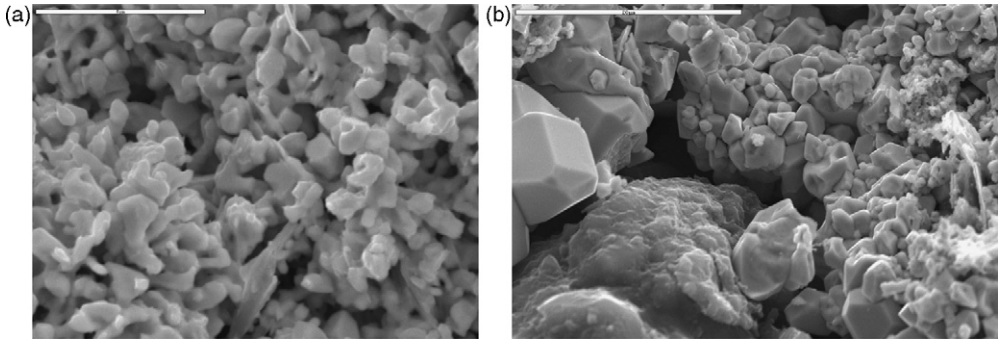

Fig. 31. Comparison of crystal morphologies of charged negative plates with 1% 2939APH graphite plus 1% of activated carbon MWV-A after formation and after 100,000 PSOC cycles. Scale bars 5 and 20 μm respectively.

Table 11
Negative plate BET changes with PSOC cycling.

Group #	Group type	BET value after formation ($m^2\ g^{-1}$)	BET value after 50k cycles ($m^2\ g^{-1}$)	BET value after 100k cycles ($m^2\ g^{-1}$)
1	2% 2939APH	0.835	0.763	0.750
6	1% 2939APH:1% N134	1.663	1.865	2.506
11	2% ABG1010	0.989	1.112	0.842
25	2% MX15	0.779	0.735	0.686
30	1% MX15:1% N134	1.765	1.886	1.571
C1	Control 1	0.784	1.079	0.775

taining 1% 2939APH graphite + 1% N134 carbon black after 50,000 PSOC cycles with lead, carbon, sulfur, cathodoluminescent and back scattered electron images The rectangles in Fig. 32 are the grid wires. The overall pattern is rather clear with dense sulfate at the bottom. The color is not uniform across the active material, showing a speckled effect. In Fig. 33 more detail is shown of the speckled areas in the charged active material where the light grey areas are clearly lead clusters. Closer examination of these speckled areas reveals lead metal clustered around graphite flakes.

Fig. 34 illustrates the chemical composition of three distinct areas imaged in the preceding figures determined using EDS (energy dispersive spectroscopy). From this it is clear that the central black speck is carbon, surrounded by lead metal.

The lead clusters can easily be seen in Fig. 32a. These are surrounded by lead sulfate as shown in Fig. 32c and d. The backscattered electron Fig. 32e again shows the lead clusters.

Fig. 34a is an EDS spectrum of a Pb-metal cluster of approximately 100 μm in length. Only Pb is present while the small C peak is due to the conductive carbon coating used to prepare the samples. Fig. 34b is an EDS spectrum of the dark grain within Pb block. Only carbon is present while the small oxygen peak (0.5 keV) is probably due to contamination. Fig. 34c is an EDS spectrum from the medium gray grain identified as $PbSO_4$. The carbon detected here is from the coating, O is due to oxygen in $PbSO_4$, and the large peak is due to both S and Pb which have almost the same X-ray energies. Compare O peak here with O peak from Pb metal in first spectrum (a). These images give additional evidence of the electrochemical reduction of Pb^{2+} ions on the carbon additive.

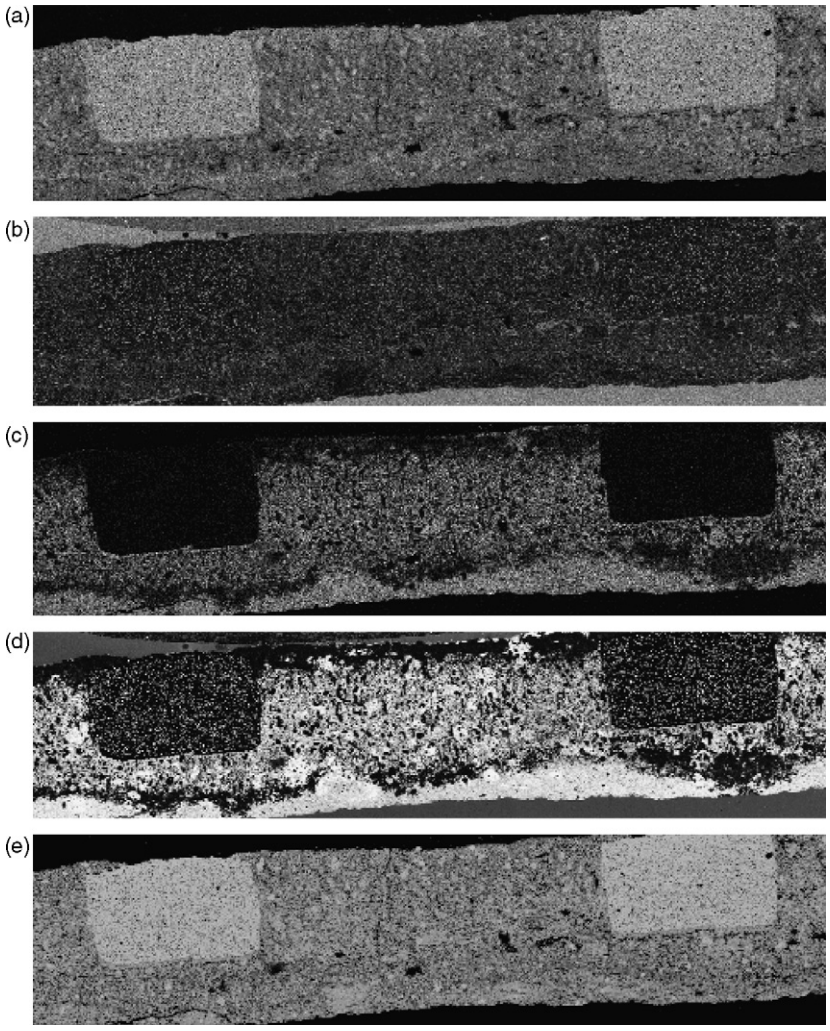

Fig. 32. Plate containing 1%2939APH graphite + 1% N134 carbon black after 50,000 PSOC cycles (a) lead, (b) carbon, (c) sulfur, (d) cathodoluminescence, (e) back-scattered electrons.

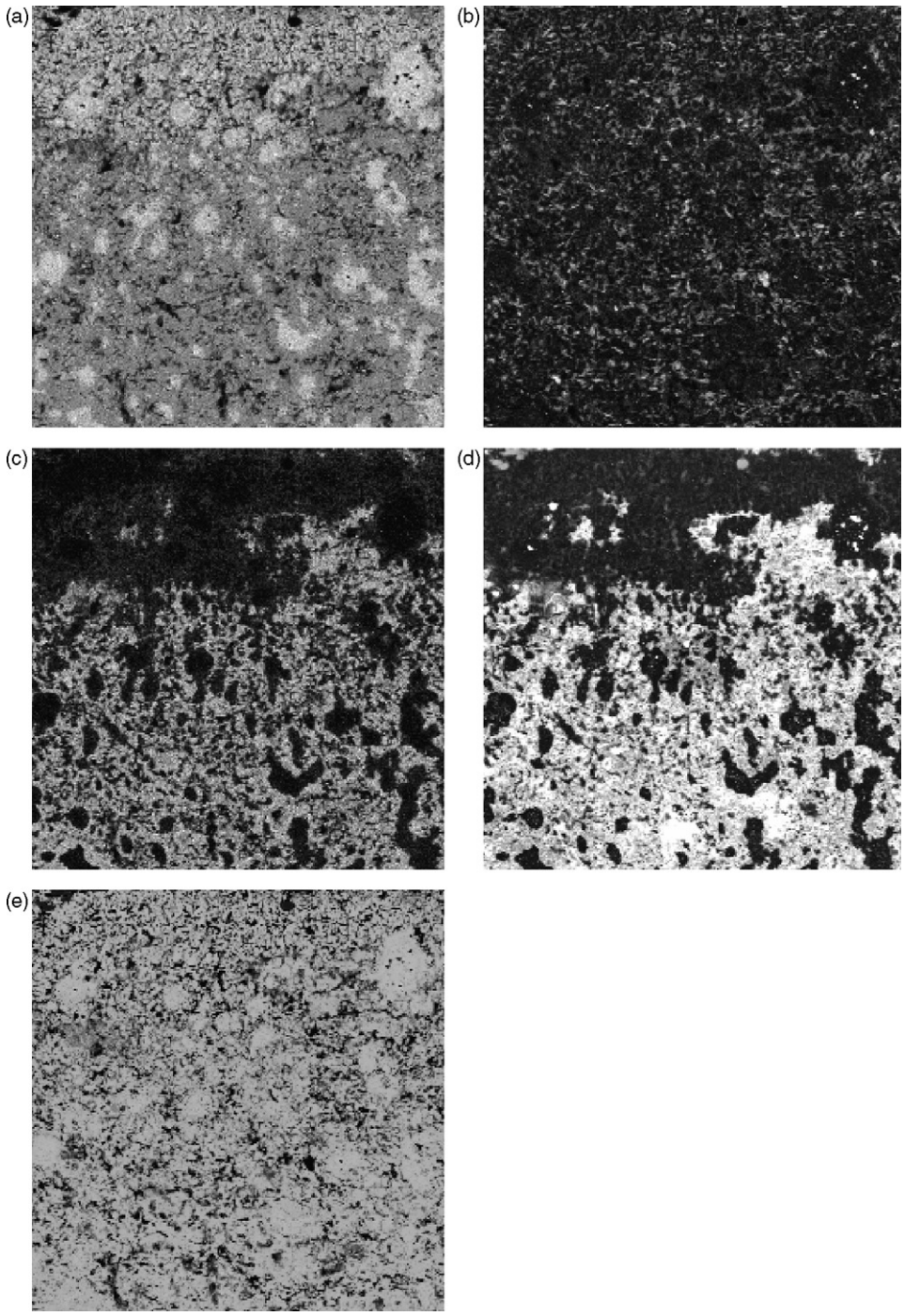

Fig. 33. Plate containing 1% 2939APH graphite + 1% N134 carbon black after 50,000 PSOC cycles (a) lead, (b) carbon, (c) sulfur, (d) cathodoluminescence, (e) back-scattered electrons. 3 μm resolution.

2.16. Discussion and conclusions

The most significant findings from Task 1 were:

(i) We have verified that the primary cause of failure of conventionally designed VRLA cells in PSOC cycling conditions is the progressive formation of inert lead sulfate that initially begins on the surface of the negative plate and then penetrates into the bulk of the active mass.
(ii) Addition of mixtures of carbon black and graphite to the NAM has a significant beneficial effect on cycle life. The best performing cells exceeded well over 100,000 cycles and failed because of factors not associated with accumulation of electrochemically inactive lead sulfate on the plate surface.
(iii) Electron microprobe imaging, coupled with cathodoluminescense shows that the problem of lead sulfate surface buildup is eliminated when carbon black/graphite mixtures are used in the NAM. Where the negative plates contained elevated levels of carbon lead sulfate was homogeneously distributed through the electrode.

Our data also show that carbon black and graphite have a significant effect on initial capacity. This probably occurs as a result of increased electrochemical efficiency of the NAM.

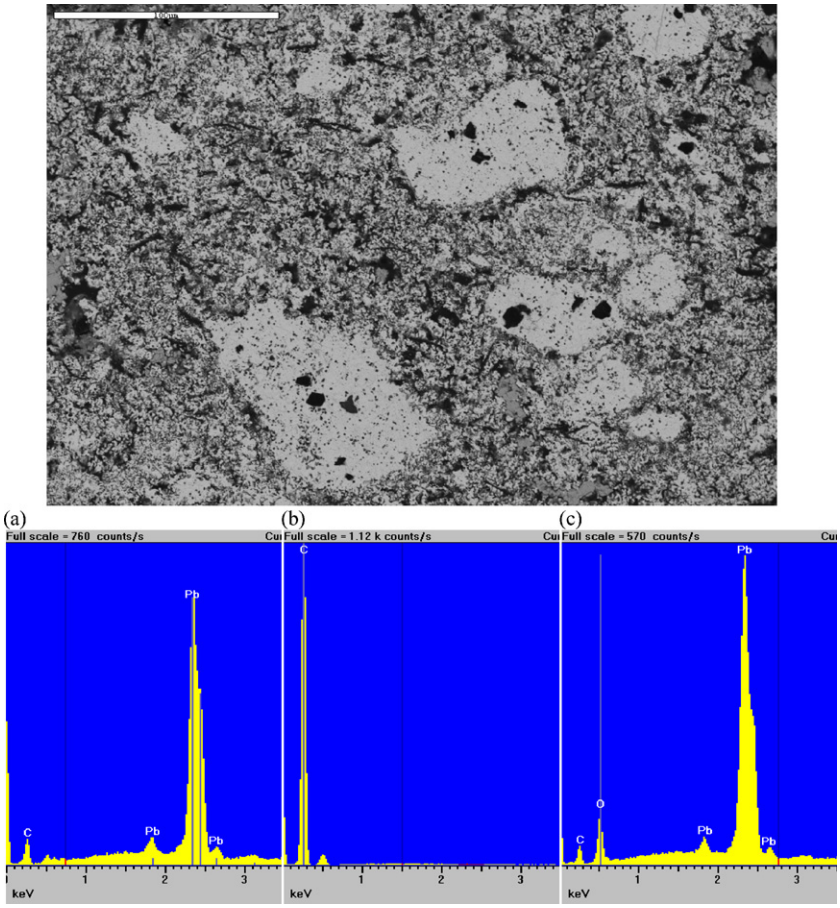

Fig. 34. Plate containing 1%2939APH graphite + 1% N134 carbon black after 50,000 PSOC cycles. BSE image showing Pb-metal clusters in fine Pb-meta matrix. Rare PbSO4 shows a medium gray (left edge; bottom edge toward right. Dark "grains" included within Pb "blocks" are carbon. Spectra from each of these grain types are shown in panels (a), (b) and (c) below.

The most significant findings from Task 2 were:

(i) We were able to confirm the beneficial effects of carbon additives in increasing the cycle life of VRLA cells in PSOC cycling operation. A wide range of carbon types was employed yet all of the test cells in Task 2 are still cycling. Some have exceeded 150,000 cycles with over 6000 capacity turnovers.

(ii) The electrical resistivity of negative active material is reduced by addition of carbon black/graphite mixtures to the paste mix. The lowest values are obtained with the ABG1010 expanded graphite and the carbon blacks N134 and Ace Black. However we should note that several of the carbon materials were used at concentrations below their percolation points therefore, in these cases, a significant reduction should not be expected.

(iii) Studies of the nucleation of lead sulfate in negative active material containing 2% carbon black and 2% graphite conclusively show that this additive eliminates the phenomenon of surface buildup and promotes nucleation in the interior of the NAM.

Given the incomplete nature of the dataset it is not yet possible to state categorically which additives perform best. In addition, dosage level studies have not been carried out in a systematic manner so we are unable to state the concentration at which the additives will be most effective. Nor have we been able to correlate the performance of the additives with their chemical and physical properties. Consequently, we cannot predict which types of carbon or which properties will give the best result. However, there are some interesting general trends.

(iv) Resistivity measurements of the additives in lead sulfate show that graphite and carbon black and their mixtures produce macro conductivity in the dosing region studied while the activated carbons did not. Unfortunately, the dosage levels employed in Task 2 were below the percolation points for most of the graphite materials so we are unable to correlate cycle life with conductivity. Dosage level studies currently underway will resolve this question.

(v) Plate preparation with high carbon concentrations causes large variations in paste density and active material specific surface area. Paste rheology is also changed significantly resulting in the need to add water to the paste mix to make it workable on conventional equipment.

(vi) In almost every case carbon additives improve both initial capacity and cycling performance relative to the control cells.

(vii) The best PSOC cycling performance is seen for mixtures containing flake graphite and carbon black. When graphite is used alone, the negative electrode polarization during high rate charging increases to the point where the battery would not accept charge during regenerative braking. When carbon black is mixed with the carbon this phenomenon is eliminated.

(viii) Electron microprobe images of plates after 50,000 cycles show the presence of lead clusters depositing around graphite particles in the active material. This indicates that soluble lead ions are electrochemically reduced on the graphite surface.

(ix) BET surface area measurements on cycled plates show a general trend to reduction of the internal surface area. Since a large fraction of the NAM surface area is due to the carbon additive this suggests that the additive is becoming progressively buried under lead and lead sulfate reaction products.

Acknowledgements

The research was sponsored by The Advanced Lead-Acid Battery Consortium, P.O. Box 12036, 2525 Meridian Parkway, Suite 100, Research Triangle Park, NC 27709-2036, USA and United States Department of Energy.

References

[1] Hollenkamp, et al., Overcoming negative plate capacity loss in VRLA batteries cycled under partial state of charge duty, ALABC Project N 1.2.
[2] R.H. Newnham, et al., Advancement of lead-acid battery technology for hybrid and electric vehicles, ALABC Project C/N 1.1.
[3] D.P. Boden, et al., ALABC Project N 4.4 "Optimization of Additives to the Negative Active Material for the Purpose of Extending the Life of VRLA Batteries in High-rate PSOC Operation", Final Report, June 2005.
[4] Murphy M., ALABC Project D. P. 1.3 Production and Test of VRLA batteries designed specifically for partial state of charge duty, Final Report, February 2007.
[5] ALABC Project No. C1.2 "Identification of the optimum specification for carbon to be included in the negative active material of a valve-regulated lead-acid battery in order to avoid the accumulation of lead sulfate during high-rate partial-state-of-charge operation", Progress Report No. 2/Annual Report: June 2007–May 2008.
[6] M. Soria, et al., ALABC Project D. P. 1.2 Production and test of VRLA batteries designed specifically for partial state of charge duty, Final Report, March 2007.
[7] N. Zakharchuck, S. Meyer, B. Lange, F. Scholz, Croatica Chemica Acta 73 (3) (2000) 667–704.
[8] U. Haase, F. Scholz, Electrochemistry Communications 3 (2001) 429–434.
[9] D. Pavlov, et al. ALABC Project C2.3 "Identification of the mechanism(s) by which certain forms of carbon, when included in the negative active material of a valve-regulated lead acid battery exposed to high-rate partial-state-of-charge operation, are able to resist sulfation", Final Report, 2009.